https://doi.org/10.5194/egusphere-2025-513
Preprint. Discussion started: 25 February 2025

Mid-Holocene sea-ice dynamics and climate in the northeastern Weddell Sea inferred from an Antarctic snow petrel stomach oil deposit

Mark A. Stevenson[1a], Dominic A. Hodgson[2,1], Michael J. Bentley[1], Darren R. Gröcke[3], Neil Tunstall[1], Chris Longley[1], Alice Graham[1], Erin L. McClymont[1]
[1]Department of Geography, Durham University, Durham, DH1 3LE, United Kingdom
[2]British Antarctic Survey, Natural Environment Research Council, Cambridge, CB3 0ET, United Kingdom
[3]Department of Earth Science, Durham University, Durham, DH1 3LE, United Kingdom
[a]Present address: Oxford Radiocarbon Accelerator Unit (ORAU), School of Archaeology, University of Oxford, Dyson Perrins Building, South Parks Road, Oxford OX1 3QY, United Kingdom

Correspondence to: Mark A. Stevenson (mark.stevenson@arch.ox.ac.uk)

Abstract. Understanding past variability in Antarctic sea ice is of critical importance to determine how it regulates global climate processes and biogeochemistry, and Southern Ocean marine ecosystems. Records of changes in Holocene sea-ice extent in the Weddell Sea is limited to a few marine sediment cores and inferences from continental ice cores. Here we present a novel record of sea-ice and climate from ~6700 – 2000 cal. yr BP based on accumulation rates and multi-proxy geochemical analyses of a snow petrel stomach-oil deposit from the Heimefrontfjella Range, Dronning Maud Land, East Antarctica. Three different sea-ice configurations are interpreted from the record. From 6700 – 6200 cal. yr BP there was a period of low sea ice cover and extensive polynyas associated with warmer temperatures and regional ice shelf retreat. From 6200 – 4700 cal. yr BP there was a gradual transition to more extensive sea-ice configuration and a switch towards foraging in coastal polynyas at the retreating ice-shelf front. Finally, between 4600 – 2000 cal. yr BP increased sea ice extent restricted access to foraging grounds which by ~6700 cal. yr BP resulted in abandonment of the nest. Our results highlight how specific Holocene sea-ice configurations can be interpreted from the geochemical composition of snow petrel stomach-oil deposits, providing insight into the interactions between oceanographic forcing, climate change, ice-shelf extent and ecosystem adaptation. We also show, for the first time, the utility of phytol and cholesterol analysis for understanding past avian diet.

https://doi.org/10.5194/egusphere-2025-513
Preprint. Discussion started: 25 February 2025

1 Introduction

Antarctic sea-ice extent is highly variable and closely coupled with continental, oceanic and atmospheric processes which both interact with and influence global climate (Brandon et al., 2010). Mechanistically, the formation of sea ice results in brine rejection which can directly contribute to the formation of Antarctic Bottom Water (AABW) (Crosta et al., 2022), helping drive ocean circulation, including the deep overturning cells (Ferrari et al., 2014) and supporting important systems such as the Weddell Gyre (Vernet et al., 2019). Upwelling can result in the formation of open ocean polynyas within the sea ice, whereas coastal polynyas are often driven by katabatic winds near the coast or ice shelf fronts (Comiso and Gordon, 1987). These polynyas can support high levels of primary productivity in the ocean (Smith et al., 2010; Sarmiento et al., 2004).

Antarctic sea-ice records reveal pronounced declines in extent since 2016, associated with recent warming (Eayrs et al., 2021), with historic lows in 2023 and 2024 (Ionita, 2024; Purich and Doddridge, 2023; Gilbert and Holmes, 2024; Nsidc, 2024; Wang et al., 2024). Improved palaeoenvironmental reconstructions of Antarctic sea ice are vital to put instrumental observations (<50 years) into a longer-term context, with projections of up to 67% decline by 2100 (Collins et al., 2013). Such reconstructions provide a historical basis to understand the interactions between climate and sea-ice extent, and interactions between sea ice and the extent of floating ice shelves and grounded ice.

Existing knowledge of Holocene Antarctic sea-ice evolution suggests there were three distinct phases, but these can be out of phase geographically due to regional responses and uncertainty associated with dating (Crosta et al., 2022). These consist of a cooler early Holocene between 11.5 ka to 8 ka BP (e.g. (Barbara et al., 2010; Etourneau et al., 2013)), followed by a warmer mid-Holocene (~7 to ~4–3 ka BP) with higher sea surface temperatures and longer ice-free summers (Crosta et al., 2022) and then a cooler late Holocene or 'neoglacial' phase ~5–3 to 1–0 ka BP marked by increased sea-ice extent as surface water temperatures reduced (Barbara et al., 2016; Taylor et al., 2001). The integration of multiple records from the Atlantic sector of the Southern Ocean suggest there was some late Holocene cooling, driven by enhanced cold-water export from the Weddell Gyre as a cavity developed under the Ronne Filchner Ice Shelf, combined with a northward shift of the Southern Hemisphere westerly wind belt (Xiao et al., 2016). However, the changes within the Weddell Sea remain poorly understood and there is a lack of data to reconstruct past sea-ice evolution (Verleyen et al., 2011), particularly over the continental shelf.

To address this, we analysed a snow petrel *(Pagodroma nivea)* stomach-oil deposit, accumulated at nesting sites in the northeastern Weddell Sea region. Such deposits have been previously demonstrated to record palaeoenvironmental information (McClymont et al., 2022; Berg et al., 2019; Ainley et al., 2006) by tracking the biochemical signature of changes in snow petrel diet, which is in turn related to environmental characteristics of their feeding grounds including sea-ice extent, and ocean productivity. Snow petrels have a close affinity with sea-ice foraging zones during the breeding season (Delord et al., 2016; Ainley et al., 2006), feeding in intermediate sea ice cover and switching between neritic (close to shore) and pelagic (offshore) feeding grounds (Ainley et al., 1998; Ainley et al., 1984) .

https://doi.org/10.5194/egusphere-2025-513
Preprint. Discussion started: 25 February 2025

Modern end-member studies have shown that specific prey species (e.g. krill, fish & squid) can be separated based on their fatty acid composition and can be used to infer different sea-ice conditions in the foraging area. For example, krill are high in $C_{14:0}$, $C_{16:0}$ and $C_{18:1}$ fatty acids [e.g. (Cripps et al., 1999)], whereas squid are dominated by $C_{16:0}$ and fish by $C_{18:0}$ fatty acids [(Lewis, 1966); reviewed in McClymont et al. (2022)]. This allows us to distinguish between an Antarctic krill-rich diet, reflecting an offshore (pelagic) habitat, and a fish-rich diet, reflecting near-shore and continental shelf environments. Sea ice composition can be interpreted in terms of the spatial distribution of fish (Ran et al., 2022; Liu et al., 2024; Freer et al., 2019), Antarctic krill (Mcbride et al., 2021) and cephalopod (mainly squid) (Xavier et al., 2016) species between coastal, shelf and offshore environments in the Southern Ocean and Weddell Sea. Stable isotopes in stomach-oils are potentially excellent indicators of ecological baseline nutrient availability, trophic status ($\delta^{15}N$) and the productivity and location of past foraging habitats ($\delta^{13}C$) (McClymont et al., 2022; Ainley et al., 2006).

Here we analyse a well-preserved snow petrel stomach-oil deposit from the Heimefrontfjella region of Dronning Maud Land, East Antarctica to reconstruct changing Holocene sea ice and climate variability in the Weddell Sea. Using a radiocarbon dated age-depth model, we analyse a range of organic geochemical biomarkers (including the first analyses of phytol and cholesterol in stomach oil deposits), bulk elemental chemistry and stable isotopes. Our record indicates three periods of distinctive Holocene climate and sea-ice cover, which we compare with existing records of environmental changes in Antarctica and the Southern Ocean ~~(Crosta et al., 2022)~~.

2 Materials and methods

2.1 Heimefrontfjella stomach oil deposit 3012MUM2 and its regional context

Stomach-oil deposit 3012MUM2 was collected in season 2014–15 from the Boysennuten nunatak in the Heimefrontfjella Range of East Antarctica (74° 34.14'S; 11° 15.02'W) (Fig. 1). The ~32 x 23 x 15 cm maximum thickness deposit had an irregular, mamillated outer surface, similar to previously sampled deposits from the wider region (McClymont et al., 2022). It was located immediately beneath a sheltered rock crevice, a typical habitat for nesting snow petrels, at an elevation of 1336 m above sea level (SI Fig.1a and 1b). It was kept in the dark and frozen at −20 °C throughout the transportation processes to Durham University where sampling was carried out from 2021. The deposit was sliced using a circular saw while still frozen to preserve the internal millimetre-scale laminae which, when oriented, spanned a depth of ~19 cm, which was slightly smaller to the maximum thickness of the deposit, due to the deposits mamillated structure and cutting on an axis to follow layering (SI Fig.1c). Sampling was carried out at 2.5 mm resolution with 3.0 mm biopsy punches for organic geochemistry, isotopes and radiocarbon analyses. A 19-cm long slice from the opposite face of the cut was mounted in plastic trunking for high-resolution X-ray fluorescence (XRF) analysis of elemental composition.

https://doi.org/10.5194/egusphere-2025-513
Preprint. Discussion started: 25 February 2025

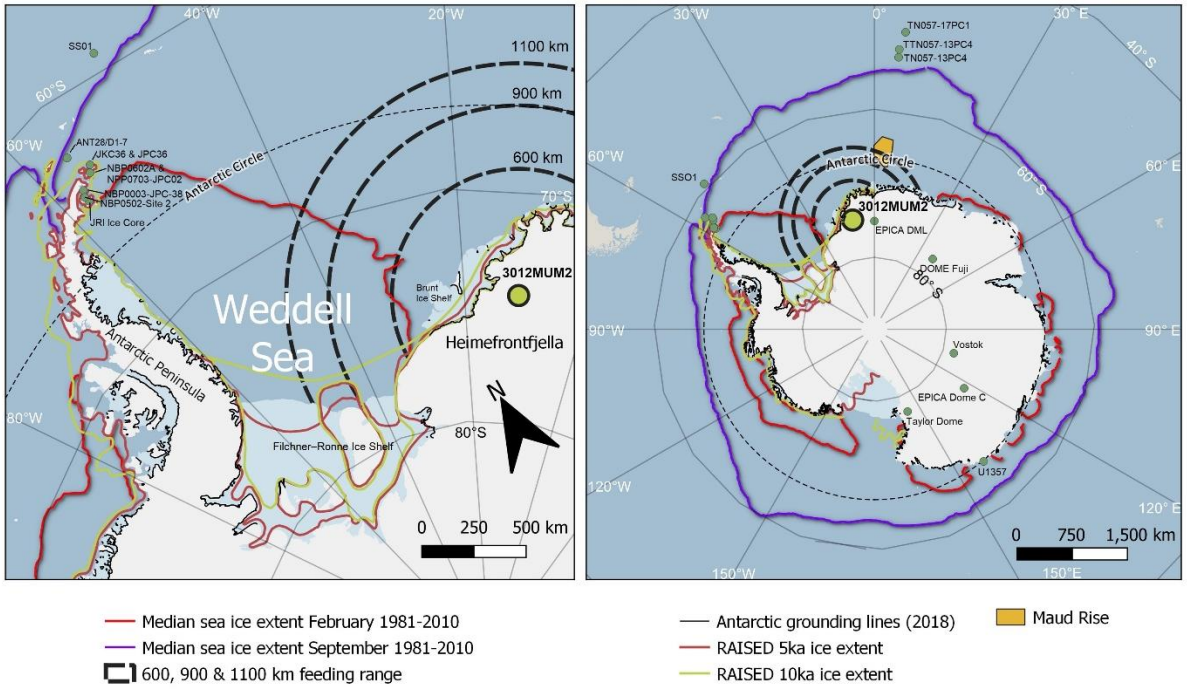

Figure 1: Location of Holocene snow petrel stomach oil record 3012MUM2, from Heimefrontfjella (74° 34.14'S; 11° 15.02'W; yellow circle) in the context of the Weddell Sea, and Antarctic Peninsula (left panel) and Antarctica and the Southern Ocean (right panel). Dashed black lines indicate sectors within 600, 900 & 1100 km snow petrel foraging range from the stomach oil deposit. Also shown are median modern sea ice extent (Fetterer et al., 2017), RAISED grounded ice sheet extents at 5ka and 10ka (Bentley et al., 2014) and inferred modern Antarctic grounding lines (Rignot, 2022). Other locations and core sites mentioned in the text include: ice cores from EPICA DML (Masson-Delmotte et al., 2011); Dome Fuji (Masson-Delmotte et al., 2011); EPICA Dome C (Masson-Delmotte et al., 2011); Vostok (Masson-Delmotte et al., 2011); Taylor Dome (Masson-Delmotte et al., 2011) and James Ross Island (JRI) (Mulvaney et al., 2012); marine sediment cores U1357 (Ashley et al., 2021); TTN057-13PC4 (Hodell et al., 2001); TN057-13PC4 (Divine et al., 2010; Nielsen et al., 2007); TN057-17PC1 (Divine et al., 2010; Nielsen et al., 2007); ANT28/D1–7 (Nie et al., 2022); NBP0003-JPC38 (Barbara et al., 2013); NBP0502-Site 2, Herbert Sound (Totten et al., 2015); NBP0602A & NPP0703-JPC02, Firth of Tay (Michalchuk et al., 2009; Majewski and Anderson, 2009); SS01 (Bak et al., 2007); and JKC36 & JPC36, Perseverance Drift (Kyrmanidou et al., 2018).

2.2 Radiocarbon analyses and age-depth modelling

An age-depth model for 3012MUM2 was constructed from twelve ^{14}C ages (Table 1). The top and bottom ages were sampled at 0 cm and 18.5 cm, immediately above and below the first geochemical samples (0.5 cm and 18.25 cm, respectively). Most of the radiocarbon ages were carried out by Beta Analytic (Miami, USA) using ^{14}C-AMS via graphitization on untreated samples. To assess for the effects of acid removal on ^{14}C ages samples at 5.0 cm and 10.5 cm were repeat-sampled at SUERC (Scottish Universities Environmental Research Centre) Environmental Radiocarbon Laboratory by digestion in 1M HCL (hydrochloric acid) (at 80 °C, 2 hours), washed free of mineral acid with deionised water, dried and homogenised. Carbon was recovered as CO_2 by heating CuO and converted to graphite by Fe/Zn reduction. Samples were then analysed by AMS at the Keck Carbon Cycle AMS Facility, University of California, Irvine, USA. For calibration of radiocarbon ages to calendar ages (Table 1) the MARINE20 radiocarbon age calibration (Heaton et al., 2020) was used taking into account the marine reservoir

https://doi.org/10.5194/egusphere-2025-513
Preprint. Discussion started: 25 February 2025

110 effect using a ΔR = 670 ± 50 years, based on the marine reservoir effect measured at Hope Bay in the western Weddell Sea (Björck, 1991b). This approach has previously been applied to snow petrel stomach-oil deposits (McClymont et al., 2022). A Bayesian age-depth model was then built in Bacon 2.3.9.1 (Blaauw and Christen, 2011). Following extensive testing, depth intervals (*d.by*) were set to 0.05, thickness to 1.2 (*thick*), accumulation rate mean (*acc.mean*) to 200, with minimum (*d.min*) and maximum (*d.max*) depth ranges set to 0 and 18.5 cm respectively. Our choice of a Bayesian approach to age-depth
115 modelling means that the age uncertainties of all dates are considered for the entire age model. This means the final age model does not necessarily pass through the central median age of each date (if calibrated individually), but instead more accurately takes into account the entire profile (Blaauw and Christen, 2011; Blaauw et al., 2023).

Table 1: Radiocarbon dates including raw ^{14}C and Bayesian calibrated ages for the 3012MUM2 sequence, together with interpolated ages
120 for top and base of samples used for biomarker/isotope sampling. Samples analysed by BETA Analytic (Florida) ^{14}C-AMS were prepared without acidification. Repeat analyses at 5 cm and 10.5 cm were prepared at SUERC Radiocarbon Laboratory using acidification and run for ^{14}C-AMS at UC Irvine Keck Carbon Cycle AMS. A reservoir offset based on closest Holocene ΔR of 670 ± 50 years (Björck, 1991a) was used, consistent with previous studies (McClymont et al., 2022) and converted to calendar ages using the MARINE20 calibration (Heaton et al., 2020).

Depth (cm)	**AMS lab ID/*deposit position information***	**Age (^{14}C yr BP)**	**± (^{14}C yr BP)**	**Bayesian modelled calibrated age using rbacon (cal. yr BP). (see Fig.2)**		
				Median	**Min**	**Max**
0.0	Beta - 679228	2510	30	1459	1134	2303
0.5	*Top of biomarker/isotope sampling*	N/A	N/A	1983	1654	2407
1.0	Beta - 620905	3520	30	2446	1901	2926
3.5	Beta - 679229	4630	30	4002	3491	4611
5.0	Beta - 620906	5030	30	4519	4158	5119
5.0	UCIAMS-276896	4958	35	4519	4158	5119
5.5	Beta - 620907	4990	30	4608	4255	5203
10.0	Beta - 620908	5520	30	5251	4908	5843
10.5	Beta - 620909	5610	30	5320	4980	5922
10.5	UCIAMS-276897	5491	35	5320	4980	5922
13.5	Beta - 620910	5910	30	5750	5396	6348
17.0	Beta - 620911	6720	30	6525	6121	7128
18.25	*Base of biomarker/isotope sampling*	N/A	N/A	6724	6332	7326
18.5	Beta - 679230	6840	30	6766	6383	7369

125

https://doi.org/10.5194/egusphere-2025-513
Preprint. Discussion started: 25 February 2025

2.3 Bulk stable isotope analysis and organic matter elemental composition

Stable isotope analysis was performed using a Costech ECS400 elemental analyser coupled to a Thermo Scientific Delta V Advantage isotope ratio mass spectrometer in the Stable Isotope Biogeochemistry Laboratory (SIBL) at Durham University. The method used is described in McClymont et al. (2022). Stable isotope analysis of carbon and nitrogen is reported in standard delta (δ) notation in per mil (‰) relative to Vienna Pee Dee Belemnite (VPDB) and atmospheric nitrogen (AIR) respectively. The linear range for $\delta^{13}C$ was between −46 ‰ and +3 ‰ and for $\delta^{15}N$ between −4.5 ‰ and +20.4 ‰, based on daily analysis of international (e.g. IAEA-600, IAEA-CH-3, IAEA-CH-6, IAEA-N-1, IAEA-N-2, NBS 19, USGS24, USGS40) and in-house standards, enabling a 2-standard-deviation analytical uncertainty of ±0.1 ‰ for international standards (replicated) and <±0.2 ‰ on replicated samples. Total carbon (wt % C) and nitrogen (wt % N) were obtained simultaneously using an internal standard of glutamic acid (40.8 wt % C; 9.5 wt % N).

2.4 Biomarker analyses

The biomarker sub-samples (0.02 – 0.05 g) were extracted in 4 mL dichloromethane (DCM):hexane (3:1) after addition of internal standards (nonadecane, heptadecanoic acid, 5α-androstane, 5α-androstanol) and then sonicated for 15 mins. Extracts were decanted and the procedure was repeated three more times. Extracts were combined and taken to dryness using rotary evaporation and N_2. The entire sample was then saponified using 1 ml KOH (8%) in methanol (95%), heated for 1 h at 70 °C and left overnight. The neutral fraction was extracted with 3 x 3 ml hexane. The remaining sample was acidified to pH <3 using drops of 2M HCL, followed by extraction of fatty acids with hexane and evaporation to dryness with N_2. Fatty acid methyl esters (FAMEs) were generated by methylating the fatty acid fraction using 3 mL methanol:HCL (95:5) heated for 12 h and left to cool. Samples were rinsed with 4M DCM-cleaned H_2O and then FAMEs were extracted with at least three DCM:hexane rinses (4:1), before evaporation to dryness under N_2. Neutral fractions were separated in up to four fractions using 4 cm deactivated silica (heated 140 °C for 16 h) columns in glass pipettes plugged with extracted cotton wool (silica pore size 60Å, 220–240 mesh particle size; 35–75 µm particle size (Sigma-Aldrich 60738-1KG)). Hexane was used to condition the columns (x3 column volumes) followed by injection of the sample dissolved in 500 µl DCM directly into the column. Elution order into separate fractions used three column volumes each of hexane, DCM, DCM:methanol (1:1) and methanol. All fractions were decanted and transferred into GC vials and evaporated to dryness using N_2. Fraction F3 (DCM:Methanol (1:1)) was then further derivatized to trimethylsilyl esters prior to analysis using 50 µl DCM and 50 µl BSTFA (N,O-Bis(trimethylsilyl)trifluoroacetamide) (with 1% TMCS (chlorotrimethylsilane)) heated for 1 h at 70 °C and left overnight prior to analysis. Samples were evaporated to dryness and dissolved in hexane prior to analysis.

All extracts were analysed using a Thermo Trace 1310 gas chromatograph coupled to an ISQ LT single quadrupole mass spectrometer (GC-MS). FAMEs extracts were separated using a Restek FAMEWAX (crossbond polyethylene glycol) column (30 m x 0.25 mm x 0.25 µm), similar to McClymont et al. (2022) but with some modifications. Briefly, samples were injected (0.8 µl) into a programmable temperature vapouring (PTV) injector in CT Splitless mode with inlet temperature at

https://doi.org/10.5194/egusphere-2025-513
Preprint. Discussion started: 25 February 2025

250 °C, carrier gas in constant flow and with helium carrier gas set to 1.5 mL min^{-1} (split flow 15.0 mL/min; splitless time 1.5 min; purge flow 5.0 mL/min). GC oven temperature was set to 100 °C for 3 min followed by 2 °C/min to 230 °C; hold of 12 min. Prep-run timeout was 10 mins and equilibration time 0.5 min. MS settings included: transfer line, 230 °C; ion source temperature, 230 °C, mass range 38 to 600 *m/z* (every 0.5 s). Compounds were identified from their respective mass spectra and retention times, with quantities calculated relative to the peak area of the internal standard heptadecanoic acid and an assumption of a 1:1 response (validated by comparison with Supelco 37 component FAME mix (CRM47885, Merck)).

Fraction F3 (previously eluted in DCM:Methanol (1:1)) was separated using a Restek Rxi-5ms (crossbond 5% diphenyl/95% dimethyl polysiloxane) column (60 m x 0.25 mm x 0.25 µm). Similarly, samples were injected (0.8 µl) into a programmable temperature vapouring (PTV) injector in CT split-less mode but at 280 °C inlet temperature, with helium carrier gas set to 2.3 mL min^{-1} set in constant flow mode (split flow set to 23 mL/min; splitless time 1 min; septum purge flow 5.0 mL/min). GC oven temperature was set to 50 °C hold for 2 min followed by 10 °C/min to 200 °C; followed by a slower ramp of 3 °C/min to 300 °C and a hold of 20 min (prep run timeout was 10 min, equilibration time 0.5 min). MS settings included: transfer line, 310 °C; ion volume, 300 °C, mass range 50 to 550 *m/z* (every 0.5 s). Compounds were identified from their respective mass spectra and retention times, with quantities of trimethylsilyl esters (TMS) calculated relative to the peak area of the internal standard 5α-androstanol and an assumption of a 1:1 response (validated by identically derivatized standard mix which included cholesterol-TMS).

2.5 XRF analyses

XRF (X-ray fluorescence) analysis was carried out at Durham University, Department of Geography using a GEOTEK XRF Core Workstation (MSCL-XYZ) equipped with a rhodium source X-ray generator with a 10 mm cross-core slit width and a 1 mm downcore window. During operation the XRF scanner was set to analyse four different beam conditions, with a counting time of 10 seconds per beam. Beam conditions applied to the generator included: (1) no filter, 10 kV; (2) 25 µm silver filter, 20 kV; (3) 125 µm silver filter, 30 kV; (4) 625 µm copper filter, 50 kV. Detector measurement of photons ranged 2–35 keV. To pre-screen complex data, including removal of missing values and selecting elemental compositions from the most appropriate beam, the R 3.6.0 package '*tidyverse'* (Wickham et al., 2019) was used to produce a master XRF dataset.

2.6 ICP-OES analysis

To determine local bedrock chemistry, a sample of rock attached to deposit 3012MUM2 was soaked in ethanol to remove stomach-oil residue (repeated 3–4 times). It was then crushed using a fly press, freeze dried for 48 hours, and ground to a fine, homogenous powder using a ball mill. Organic matter was removed by adding 4 ml of 30% hydrogen peroxide to a ~0.5 g aliquot of rock. The sample was then digested for 4 hours in 16 ml of Aqua Regia using a DigiPREP digestion block, and subsequently diluted to 50 ml with deionised water and filtered at 0.45 µm. Elemental composition was determined using an Agilent Technologies 5100 Inductively Coupled Plasma Optical Emissions Spectrometer (ICP-OES).

https://doi.org/10.5194/egusphere-2025-513
Preprint. Discussion started: 25 February 2025

2.7 Statistical and numerical analyses

Cluster analysis was carried out to highlight changes in geochemistry between neighbouring units in both inorganic (XRF) and organic (stable isotopes, TOC, C/N ratio and biomarkers) parameters down sample. For each dataset (organic (Org 1-3) and inorganic (XRF 1-3), separately) a constrained hierarchical cluster analysis based on sample order was performed using the *rioja* package in *R* (Juggins, 2020) and compared with the broken stick model of random zones (Bennett, 1996) to identify the maximum number of statistically significant clusters.

Principal components analysis (PCA) was carried out in Canoco V.5.51 (Ter Braak and Smilauer, 2002) on $\log_{10}$-transformed and centred data: the inorganic (XRF) and organic (bulk organic geochemistry and biomarkers) parameters were treated separately. As most XRF parameters had samples with counts <500 we chose to retain all parameters that had passed the pre-screening process (see section 2.5 XRF analyses).

3 Results

3.1 Stomach-oil deposit 3012MUM 2 age model

The stomach-oil deposit 3012MUM2 spans the interval of 1459 (1134–2303) cal. yr BP at 0 cm and 6766 (6383–7369) cal. yr BP at 18.5 cm (Table 1, reconstructed model, Fig. 2a). Biomarker and isotope samples were not taken over as full a range as the ^{14}C samples due to characteristic deposit plasticity at its margins and so we note the oldest and youngest biomarker and isotope samples lie at 0.5 cm (1983 (1654–2407) cal. yr BP) and 18.25 cm (6724 (6332–7326) cal. yr BP) respectively in the Bayesian model, which we here summarise as ~2000 to 6700 cal. yr BP. The accumulation rate based on the median Bayesian modelled age between radiocarbon dating depths varied between 10.1 and 70.0 mm kyr^{-1} (Fig. 2b).

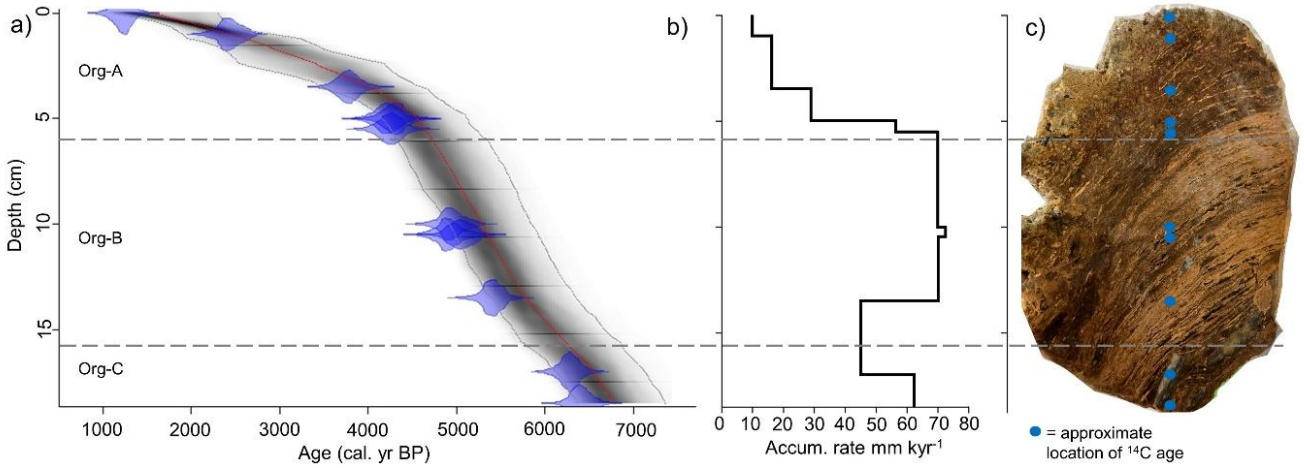

Figure 2: a) Bayesian ^{14}C-AMS age-depth model for stomach oil deposit 3012MUM2, generated in Bacon v2.3.9.1 (Blaauw and Christen, 2011) applying a reservoir offset ($\Delta R^{\text{Holocene}}$ 670 yr ± 50 years (McClymont et al., 2022)), calibrated to calendar ages using MARINE20 (Heaton et al., 2020). b) accumulation rate between age control points calculated from median ages in the Bayesian model in (a). c) photograph of stomach oil deposit 3012MUM2 after sectioning, complete with approximate location of ^{14}C ages in blue dots. Constrained

https://doi.org/10.5194/egusphere-2025-513
Preprint. Discussion started: 25 February 2025

hierarchical cluster analysis was used to determine three significant clusters (Org A-C) using organic parameters in rioja (Juggins, 2020), compared with the broken-stick model (Bennett, 1996).

3.2 Compositional changes in bulk organic matter and stable isotopes

Similar to previously measured snow petrel stomach-oil deposits [e.g. (McClymont et al., 2022; Berg et al., 2023; Hiller et al., 1988)] 3012MUM2 samples were high in organic C (36.6 – 68.3% (mean 49.8%)) and total N (2.9 – 16.8% (mean 9.7%) (Fig. 3). The $C:N_{atomic}$ ratio varied between 3.4 and 20.8 (mean 7.5). Bulk $\delta^{13}C$ had a narrow range from −31.0 ‰ to −29.5 ‰, with a mean of −30.3 ‰ and a very small standard deviation (SD) of 0.3 ‰ (Fig. 3), within the range of previous measurements of a Holocene deposit (Ainley et al., 2006). In contrast bulk $\delta^{15}N$ had a wide range between 9.3 ‰ and 19.1 ‰ (mean 9.3 ‰, SD 1.6 ‰) (Fig. 3).

3.3 Compositional changes in biomarkers

3012MUM2 deposit samples likely comprised predominately wax esters consistent with existing stomach oil studies (Imber, 1976; Lewis, 1966, 1969; Warham et al., 1976; Watts and Warham, 1976), although some may have already existed as free lipids. Once saponified and derivatised the extracts were rich in fatty acids (FA) and alcohols (FAlc) (Fig. 3; SI Fig. 3). Diagnostically these fatty acids (FA) are commensurate with previous stomach-oil and source end-member studies which suggest a diet of krill (mainly $C_{14:0}$ (FA), $C_{16:0}$ (FA)), squid ($C_{16:0}$ (FA)) and fish ($C_{16:0}$ (FA), $C_{18:1}$ (FA)) (Cripps et al., 1999; Lewis, 1966) summarised in McClymont et al. (2022) and further explored in Berg et al. (2023). In 3012MUM2, $C_{16:0}$ was the most abundant fatty acid (mean 38.9% ± 8.8% SD), followed by $C_{18:1}$ (FA) (mean 23.6% ± 10.9% SD), $C_{14:0}$ (FA) (mean 22.1% ± 5.2% SD), $C_{18:0}$ (FA) (mean 8.4% ± 2.1% SD) and $C_{16:1}$ (FA) (mean 7.1% ± 3.5% SD).

By concentration, FA were most abundant (total mean 59021.6 µg g^{-1} TOC, SD 30125.2 µg g^{-1} TOC) followed by key *n*-alcohols (FAlc) (mean 4071.1 µg g^{-1} TOC, SD 3210.5 1 µg g^{-1} TOC). The other compounds were less abundant, with cholesterol the highest (mean 757.7 1 µg g^{-1} TOC, SD 429.6 1 µg g^{-1} TOC) and phytol in lower concentrations (mean 24.7 1 µg g^{-1} TOC; 14.0 1 µg g^{-1} TOC). Phytol is formed from the ester-linked side chain of chlorophyll-*a* and can therefore primarily be considered a biomarker for phytoplankton (Rontani and Volkman, 2003). Cholesterol is a ubiquitous marker but in this context could be considered a krill marker (both Antarctic and ice krill), since it can account for more than 76% of total sterols in krill (Ju and Harvey, 2004) and is typically lower in concentration in fish. We also assessed the distributions of sterols (e.g 22-dehydrocholesterol), stanols (e.g. coprostanol) and cholesterol derivatives (e.g cholesterol α/β-epoxide), with cholesterol the most abundant contributor (SI Fig. 4).

During saponification of the relevant wax esters, *n*-alkanols (FAlc) were also formed with saturated even chain lengths; $C_{14:0}$ (FAlc) to $C_{22:0}$ (FAlc) *n*-alcohols were the most abundant (SI Fig. 3). Amongst the *n*-alcohols $C_{16:0}$ (FAlc) was the most abundant (mean 63% ± 2.9 % SD), followed by $C_{14:0}$ (FAlc) (mean 22.4% ± 1.8 % SD) and $C_{18:0}$ (FAlc) (mean 13.0% ± 2.1% SD). $C_{20:0}$ (FAlc) (mean 1.3% ± 0.4% SD) and $C_{22:0}$ (FAlc) (mean 0.3% ± 0.1% SD) *n*-alcohols were relatively minor contributors.

https://doi.org/10.5194/egusphere-2025-513
Preprint. Discussion started: 25 February 2025

Broadly, PC axis 1 for the organic geochemistry indicators had high positive loadings in C:N ratio and $C_{18:0}/C_{18:1}$ (FA), while PC axis 2 had strong positive loadings in $C_{16:0}$ (FA), $C_{18:0}$ (FA), $\delta^{15}N$ and C:N ratio (SI Table 2 & SI Fig. 8).

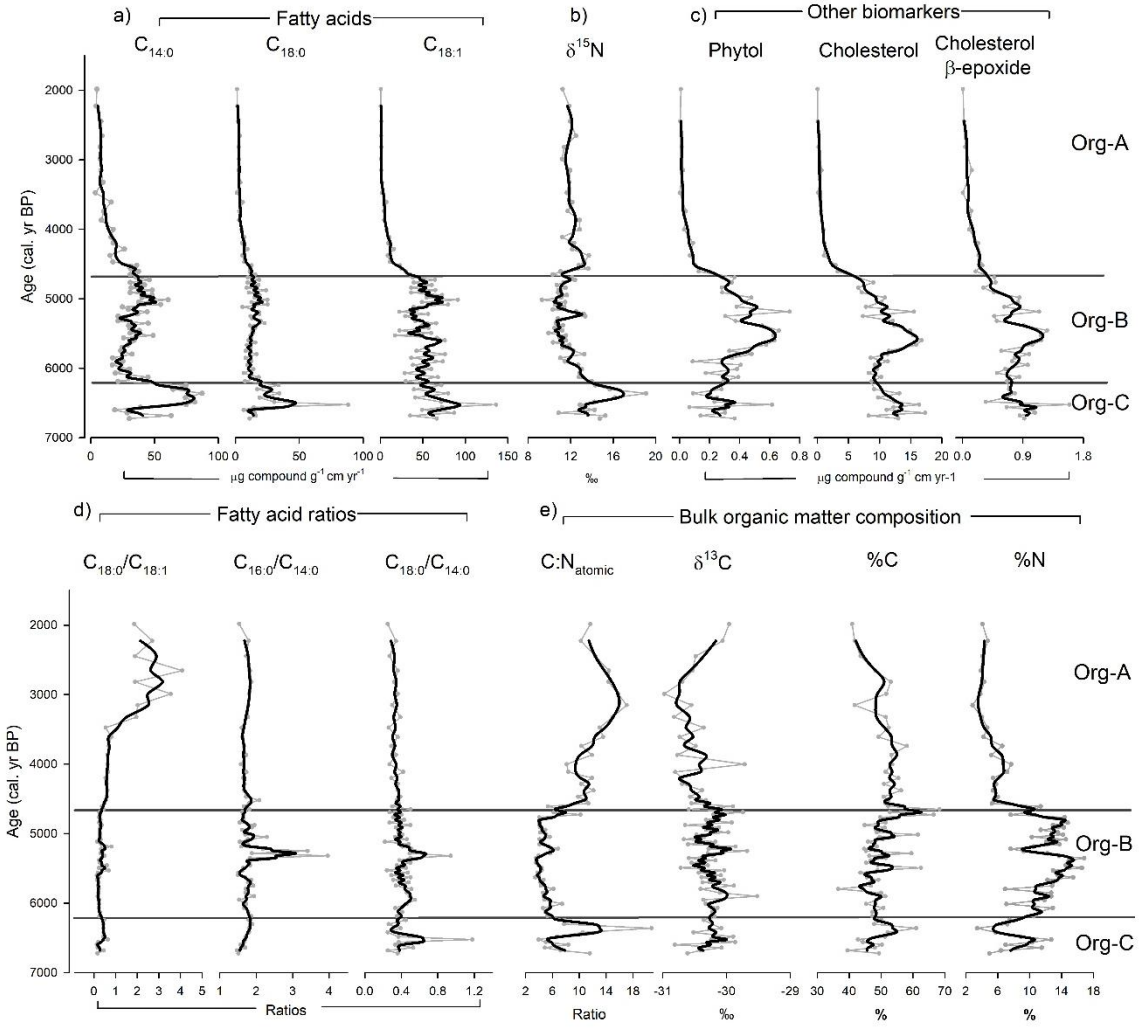

Figure 3: Organic parameters as fluxes and ratios measured in stomach oil deposit 3012MUM2, plotted against the age-depth model (Fig.2). Smooth lines in bold are 3-point moving averages. Constrained hierarchical cluster analysis was used to determine three significant clusters (Org A-C) using organic parameters in rioja (Juggins, 2020), compared with the broken-stick model (Bennett, 1996). a) Fatty acid concentrations ($C_{14:0}$, $C_{18:0}$, $C_{18:1}$); b) nitrogen stable isotopes ($\delta^{15}N$); c) Other biomarkers (phytol & cholesterol); d) Fatty acid ratios ($C_{18:0}/C_{18:1}$, $C_{16:0}/C_{14:0}$, $C_{18:0}/C_{14:0}$); e) other measures of bulk organic matter composition ($C:N_{atomic}$ ratio, $\delta^{13}C$, %C and %N).

3.4 Changes in biomarkers through time

Cluster analysis identified three statistically significant organic zones (Org-A, B & C) which are used as a framework to discuss the changes in key biomarkers through time.

https://doi.org/10.5194/egusphere-2025-513
Preprint. Discussion started: 25 February 2025

3.4.1 Organic Zone – C (~6700 – 6200 cal. yr BP)

The base of this deposit is marked by relatively high fatty acid (FA) fluxes: $C_{14:0}$ (FA), $C_{18:0}$ (FA) and $C_{18:1}$ (FA) increased to maxima around ~6400 cal. yr BP and remained high to the top of the zone (6216 cal. yr BP) (Fig. 3). This is broadly coincident with a pulse of high $\delta^{15}N$ (reaching ~20 ‰), which follows the trend in $C_{14:0}$ (FA) most closely (Fig.3). Ratios of fatty acids $C_{18:0}/C_{18:1}$ (FA) and $C_{16:0}/C_{14:0}$ (FA) remained low, with a pulse in $C_{18:0}/C_{14:0}$ (FA) reaching a maximum at ~6500 cal. yr BP (Fig. 3). A peak of 60% C ~6100 cal. yr BP is reflected in the maximum $C:N_{atomic}$ ratio value of ~21 (Fig 3). $\delta^{13}C$ fluctuated between −29.9 ‰ and −30.8 ‰. Phytol and cholesterol were relatively high with phytol fluctuating between 0.06 and 0.6 µg g^{-1} cm yr^{-1} and cholesterol between 0.3 and 1.6 µg g^{-1} cm yr^{-1} (Fig. 3). All *n*-alkanols (FAlc) increased to higher concentrations around ~6500 cal. yr BP (SI Fig. 3). Most other biomarkers of sterols, stanols and cholesterol derivatives were generally high in this zone (SI Fig. 3). Organic PC 1 was low, but PC 2 increases to high values reflecting the contributory effect of $C_{14:0}$ (FA) and $\delta^{15}N$ for PC 2.

3.4.2 Organic Zone – B (6200 – 4700 cal. yr BP)

The transition to zone B (~6200 cal. yr BP) is marked by a rapid decrease in $C_{14:0}$ (FA), $C_{16:0}$ (FA) and $C_{18:0}$ (FA) fatty acid fluxes which thereafter remained broadly stable throughout the zone (Fig. 3; SI Fig. 2). Zone B has markedly lower $\delta^{15}N$ (fluctuating between ~8 and 10 ‰). In contrast, the $C_{16:1}$ (FA) and $C_{18:1}$ (FA) fatty acid concentrations decreased from around 5400 cal. yr BP to the top of zone B, which is also observed in phytol and cholesterol from ~5300 cal. yr BP (SI Fig. 2 & 3). Notably, the flux of fatty acids did not show a decline to the top of the zone, but remained fluctuating, with further peaks at ~5600 and 5000 cal. yr BP (Fig. 3). The major *n*-alkanols were markedly lower in zone B compared to zone C (SI Fig. 3), with a similar trend to lower values in $C:N_{atomic}$ ratio (Fig. 3). Notably, at ~5200 cal. yr. BP there is a short-lived unusual interval of high $\delta^{15}N$, high $C_{16:0}/C_{14:0}$ (FA), $C_{18:0}/C_{14:0}$ (FA) and a small increase in C:N ratio (Fig. 3). Both $\delta^{13}C$ (fluctuating ~ −30.7‰ to −29.5‰) and %C (fluctuating ~ 36.6 % to 66 %) were variable at this time (Fig. 3). Other biomarkers of sterols, stanols and cholesterol derivatives were generally high at the bottom of this zone (6200 cal. yr BP), typically decreasing by the top (~ 4700 cal. yr BP) (SI Fig. 4). Organic PC1 remains low ~600 cal. yr BP, increasing slightly by the top of the zone (~4700 cal. yr BP), while PC2 is markedly lower throughout compared with zone C (SI Fig. 2).

3.4.3 Organic Zone – A (4700 – 2000 cal. yr BP)

For most biomarkers zone A is a relatively stable period, with fluxes and concentrations of $C_{14:0}$ (FA), $C_{18:0}$ (FA) and $C_{18:1}$ (FA) remaining low, broadly similar to the previous zone B and $C_{16:0}/C_{14:0}$ (FA) and $C_{18:0}/C_{14:0}$ (FA) stable throughout (Fig. 3; SI Fig. 2 & 3). Between 4250 and 4550 cal. yr BP $\delta^{15}N$ was slightly higher (reaching 13.7 ‰) before decreasing towards the top of the deposit (Fig. 3). $C_{14:0}$ (FAlc), $C_{16:0}$ (FAlc) and $C_{18:0}$ (FAlc) *n*-alkanols also reached maxima at ~4000 cal. yr BP (SI Fig. 3). $C_{16:1}$ (FA) and $C_{18:1}$ (FA) concentrations were markedly lower than zone B, and decreased further to the top of zone A (SI Fig. 2 & 3), with a similar trend in $C_{18:1}$ (FA) fluxes (Fig. 3). Of note, after ~3200 cal. yr BP $C_{18:0}/C_{18:1}$ (FA) ratios increased,

https://doi.org/10.5194/egusphere-2025-513
Preprint. Discussion started: 25 February 2025

and reached a maximum of ~4 at 2800 cal. yr BP. Similarly, $C:N_{atomic}$ gradually increased to a maximum of ~17 by ~3100 cal. yr BP, before decreasing to the top of the sequence (~ 11.7), while $\delta^{13}C$ displayed the reverse trend (increasing from ~ −31 ‰ at ~2800 cal. yr BP to −29.9 ‰ at the top of the sequence) (Fig. 3). Phytol and cholesterol were relatively low in zone A, and both displayed trends of decreasing concentrations to the top of the sequence (Fig. 3). Other biomarkers of sterols, stanols and cholesterol derivatives were similarly also low throughout zone A (SI Fig. 4). In zone A PC1 increases markedly throughout the zone, reflecting the increasing importance of C:N ratio and $C_{18:0}/C_{18:1}$ (FA) (SI Fig. 2).

3.5 Inorganic composition (XRF)

Cluster analysis identified three major XRF clusters: XRF-C (6766–4904 cal. yr BP); XRF-B (4904–4496 cal. yr BP); XRF-A (4496–1983 cal. yr BP). Zone XRF-C broadly coincides with organic zone C and B, with XRF-B aligning with the uppermost part of organic zone B. Zones XRF-A and organic zone A are broadly aligned.

Based on XRF mean counts per second (CPS) the largest elemental contributors to stomach-oil deposit 3012MUM2 were Cl, Ca, Fe, S, K, Br and P. Elevated Fe, Al, Mg and Ca in the rock specimen taken from 3012MUM2 (SI. Table 3) suggest that these elements have a locally-derived erosional contribution. Other elements potentially in part may derive from windblown particulates (Cl, S, Br and P) (Fig. 4, SI. Fig 5 & 6). Cu was also present which is known to be a key Antarctic krill marker as a Cu backbone structure is found in hemocyanin (Bridges, 1983).

Key XRF-derived inorganic compositions are presented in Fig. 4. Fe reflects a group of elements with high contributions to PC 1 (reflecting 28% of variance (SI Table 1; SI Fig. 9)) which are characterised by a peak in XRF-C ~6500 cal. yr BP, followed by declines to ~6000 cal. yr BP. Values then gradually increase to a further peak ~4000 cal. yr BP and remain stable to the top of the core. We posit Ca as an element driven by local erosion which has some similarities to PC1 but is marked by elevated values within zone XRF-B and an overall decline in XRF-A.

Cl reflects a group of compounds with high contributions to PC 2 (reflecting 22% of variance. PC2 is characterised by declines in XRF-B to minimum values at the start of XRF-A. Changes in PC 2 primarily reflect positive loadings in S and Cl (SI Table 1; SI Fig. 9) but negative loadings from elements which are commonly associated with seabirds (e.g. P, Zn, Sr, Ni), including Cu (Shatova et al., 2016; Shatova et al., 2017; Castro et al., 2021; Sparaventi et al., 2021) which supports our interpretation of an Antarctic krill marker. Broadly elevated Cu in organic zone B (with elevated $C_{14:0}$ FA and cholesterol) and low values for both in organic zone A support this interpretation, but we note that only Cu and cholesterol show comparable patterns in organic zone C. Cholesterol also tends to be a major component of guano (Cheng et al., 2016). We posit P and S as indicative of bird guano (Tatur et al., 1997; Roberts et al., 2017; Sun et al., 2000; Liu et al., 2005) and so likely to reflect prey, while Br has the potential to be windblown (Hughes et al., 2012). The relationship between nitrogen and minerogenic elements suggests some N has a guano origin given negative relationship between C:N and other elements (Cl, P, S) (SI Fig. 7) consistent with other studies (Berg et al., 2019; Hiller et al., 1988), but in contrast with a record from Marine Isotope Stage 3 (McClymont et al., 2022). A positive correlation between P and N also support a guano signal for these elements (SI Fig. 8). Bedrock contamination is unlikely given local gneiss bedrock (SI Table 3).

https://doi.org/10.5194/egusphere-2025-513
Preprint. Discussion started: 25 February 2025

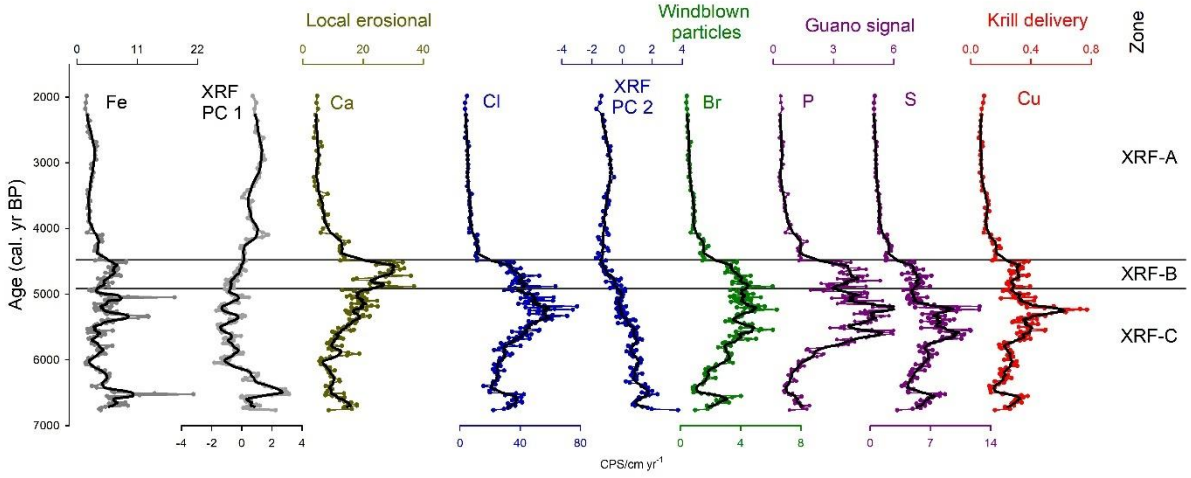

Figure 4: Key inorganic elements measured in stomach-oil deposit 3012MUM2, plotted as qualitative counts per second (cps) normalised to accumulation rate, to approximate element fluxes against the age-depth model (Fig. 2). Elements includes Fe, XRF-PC1, Ca, Cl, XRF-PC2, Br, P & S. Plots are coloured according to PCA axes and our environmental interpretations: grey = positive scores on PC axis 1, blue = positive scores on PC axis 2, teal = local erosional, green = windblown particles, guano signal = purple & red = potential krill delivery. Black lines indicate 7-point moving averages. Cluster boundaries (XRF-A, B & C) and XRF PCA are uniquely calculated from entire XRF dataset (Figure SI Fig. 3).

4 Discussion

We found pronounced variations in geochemical proxies in stomach-oil deposit 3012MUM2 spanning much of the Holocene [~ 6724 – 1983 cal. yr BP (Bayesian modelled median age range)]. Given the dependence of snow petrel dietary composition on environmental conditions this indicates that the Weddell Sea changed markedly through the Holocene in terms of sea-ice extent and distribution, ocean productivity and climate. These changes are a result of the interactions between water mass upwelling, solar forcing, wind strength (including position of southern westerlies) and the moderating effect of expanding or contracting ice sheets (Denis et al., 2010; Hillenbrand et al., 2017).

4.1 Role of ice shelf retreat on the accessibility of foraging areas

In the Weddell Sea region, deglacial ice-sheet thinning and retreat continued after ~8 ka (Nichols et al., 2019; Johnson et al., 2019), whereby retreat of the Filchner and Ronne Ice Shelf was known to have been completed by 7.7 ^{14}C corrected kyrs BP on the inner shelf (Hillenbrand et al., 2017), corroborated by ice core sodium analyses (Grieman et al., 2024). Additionally, Brunt Ice Shelf geophysical investigations supports the general picture of sustained retreat until at least 8351 cal. yr BP (Hodgson et al., 2018). Maintenance of the ice fronts in a retreat scenario from the start of the record is consistent with our evidence of increased availability of productive foraging habitat. More widely, the transition to cooler temperatures was probably characterised by mid-Holocene ice shelf cavity expansion, which led to cooling of surface waters and expansion of sea ice, which in-turn slowed basal melting at the ice-sheet margin (Ashley et al., 2021).

https://doi.org/10.5194/egusphere-2025-513
Preprint. Discussion started: 25 February 2025

4.2 Interpreting changes in sea ice in mid-Holocene stomach-oil deposits

The evolution of Holocene sea ice has been separated into three distinct phases around Antarctica (Early Holocene ~11.5 to ~8 ka BP; mid-Holocene ~7 to ~ 4-3 ka BP; the late Holocene ~5-3 to 1-0 ka BP), with the phasing of these periods differing depending on regional response to long-term forcing (Crosta et al., 2022). Here we explore how each of the three statistically significant geochemical zones in the stomach oil deposit align with the timing or direction of the environmental shifts recorded by Crosta et al. (2022) and similar studies elsewhere in Antarctica.

Our conceptual diagrams (Fig. 5) highlight how we use the geochemical evidence of three zones in the stomach oil deposits to infer changes in ~~of~~ sea-ice extent and other oceanographic parameters. In Organic zone C (6700–6200 cal. yr BP) the snow petrel stomach oil accumulation rate was high with geochemical evidence of a diet high in both fish (evidenced by FA $C_{18:0}$) and Antarctic krill *(Euphausia superba)* (evidenced by FA $C_{14:0}$). Zone C has a short interval of high productivity indicators, which we interpret as a relatively reduced sea-ice extent with intermediate sea-ice concentration, so that open waters (polynyas) were readily accessible for foraging and is most similar to present-day conditions (Fig. 3; Fig 5a). The second period is detailed by organic zone B (6200–4700 cal. yr BP) and features continued contribution of Antarctic krill *(Euphausia superba)* to the diet ($C_{14:0}$ (FA), cholesterol, Cu) which indicates that foraging was possible beyond the continental shelf edge, but lower fluxes in krill and fish markers (FA $C_{14:0}$ and $C_{18:0}$) and gradually declining FA $C_{18:1}$ (mostly krill, but some fish) (Fig. 3) compared to organic zone C suggest that this may have been more intermittent. We therefore propose organic zone C as a gradual transition sea-ice scenario (Fig. 5b) whereby there was a switch to more coastal (neritic) feeding grounds rich in fish and ice krill, but in slightly less abundance than organic zone C, despite high primary productivity (Fig. 3). We hypothesise that the biogeochemical evidence in organic zone B is consistent with foraging in both open waters within the sea ice (polynyas), which could include at the ice-shelf front, and occasional feeding at the sea-ice edge when foraging range permits. Finally, lower concentrations in most organic proxies and low fluxes of all components to the deposit as accumulation rate falls (Fig. 2–4) is evidenced by a cooler or neoglacial phase organic zone A (4700–2000 cal. yr BP) (Fig. 5c) which is characterised by more extensive sea ice which limited snow petrel foraging.

https://doi.org/10.5194/egusphere-2025-513
Preprint. Discussion started: 25 February 2025

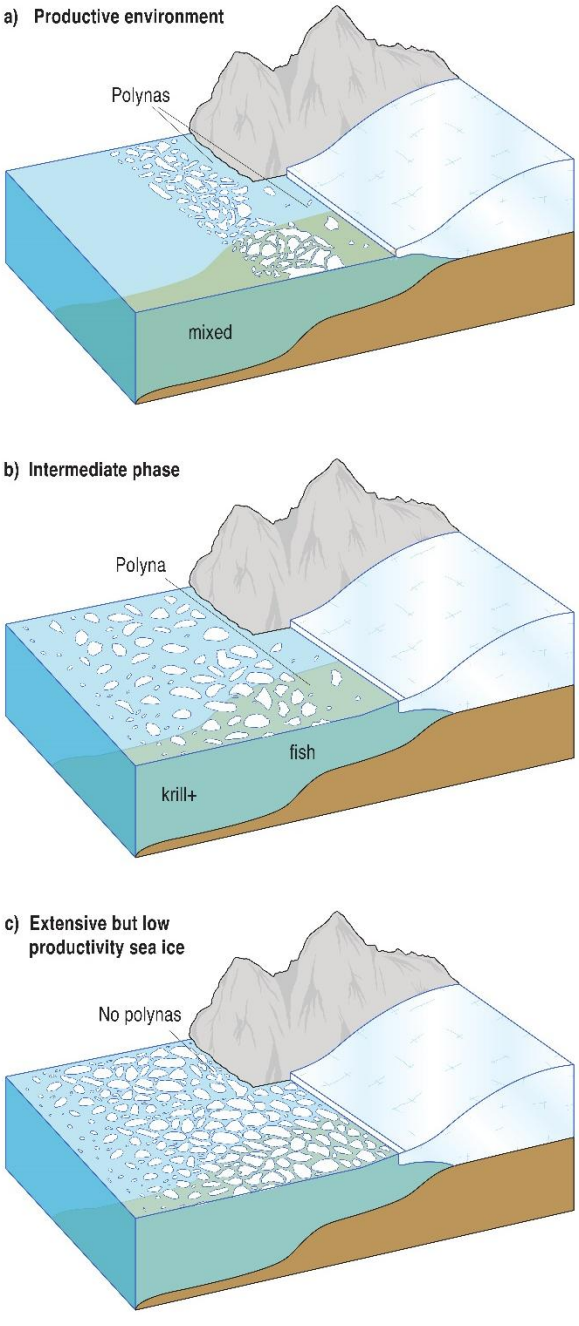

Figure 5: Conceptual diagrams highlighting Antarctic Weddell Sea ice environments interpreted for the three stratigraphic zones in the stomach-oil deposit 3012MUM2 biomarker record. a) Indicates a productive environment similar to current present-day ice scenario, with a reduced sea-ice extent with intermediate sea ice concentration. For snow petrels this period has more accessible open water with minor sea ice to enable feeding (e.g. zone org-C); b) Indicates an intermediate sea-ice configuration inferred from a switch to more coastal feeding grounds. In this scenario feeding will occur in localised polynyas as well as occasional feeding at the sea-ice edge where foraging range permits (e.g. zone org-B); c) Indicates a more extensive sea-ice and low productivity environment where feeding is blocked by extensive ice (e.g. zone org-A).

https://doi.org/10.5194/egusphere-2025-513
Preprint. Discussion started: 25 February 2025

4.3 Coherence with other records of Holocene environmental changes in the Weddell Sea

Our records show a clear match between our snow petrel stomach oil deposit and proxy records in the wider Weddell Sea region, likely due to both regions being influenced by proximity to the Weddell Gyre climate zone and atmospheric processes that determine sea-ice configurations. Consistent with high dietary fatty acid concentrations in our Heimefrontfjella record (organic zone C, 6700–6200 cal. kyr BP) (Fig. 3 & 6), the HBI (highly branched isoprenoid) sea-ice record from the Vega Drift (JPC 38; Fig. 1) features a reduction in sea-ice conditions from around 7.4 ka BP (Barbara et al., 2016) (Fig. 6). A more productive and open-ocean type sea ice configuration was reached by 7.2 cal. kyr BP at Herbert Sound and Croft Bay, and suggests mid-Holocene warming (e.g. core NBP0502-Site 2) (Totten et al., 2015). In the Firth of Tay (Fig. 1), the mid-Holocene climatic optimum spans 7800–6000 cal. yr BP (core NBP0602A) (Michalchuk et al., 2009) and 7750 and 6000 yr BP (cores NBP0602A-8B and NBP0703-JPC02) (Majewski and Anderson, 2009), was attributed to seasonally-open marine conditions. Scotia Sea diatom records were also in phase with our results, with seasonally open water assemblages from 8300 to 2400 yr BP (core SS01) (Bak et al., 2007).

Consistent with gradual transition organic zone B, the biomarker and diatom record at Vega Drift (core JPC38) shows a clear shift to cooler temperatures at ~5 ka BP and associated expansion of the Weddell Gyre (Barbara et al., 2016). At Bransfield Strait (core D1-7) persistent sea ice is observed between 5.8 and 3.8 ka BP (core ANT28/D1–7) (Nie et al., 2022), providing evidence of gradually increasing sea-ice extent.

The neoglacial, sea-ice expansion and cooling phase in organic zone A is inferred from reduced stomach oil accumulation rates and reduced concentrations of multiple organic markers in the deposit (Fig 3 & 6). The switch to reduced productivity is coherent with a sediment record on the Firth of Tay (core NBP0602A-8B and NBP0703-JPC02) which shows cooling from ~3500 yr BP based on foraminifera records (Majewski and Anderson, 2009). At Perseverance Drift, the warm interval persists longer than in our deposit, with high abundance of the foraminifera *Globocassidulina* spp. between 3400 and 1800 yr BP indicating incursions of Weddell Sea Transitional Water and a period of 'freshening' consistent with open-marine or seasonally open marine conditions, followed by its absence from ~1800 yr BP (Kyrmanidou et al., 2018) (cores JKC36 and JPC36).

https://doi.org/10.5194/egusphere-2025-513
Preprint. Discussion started: 25 February 2025

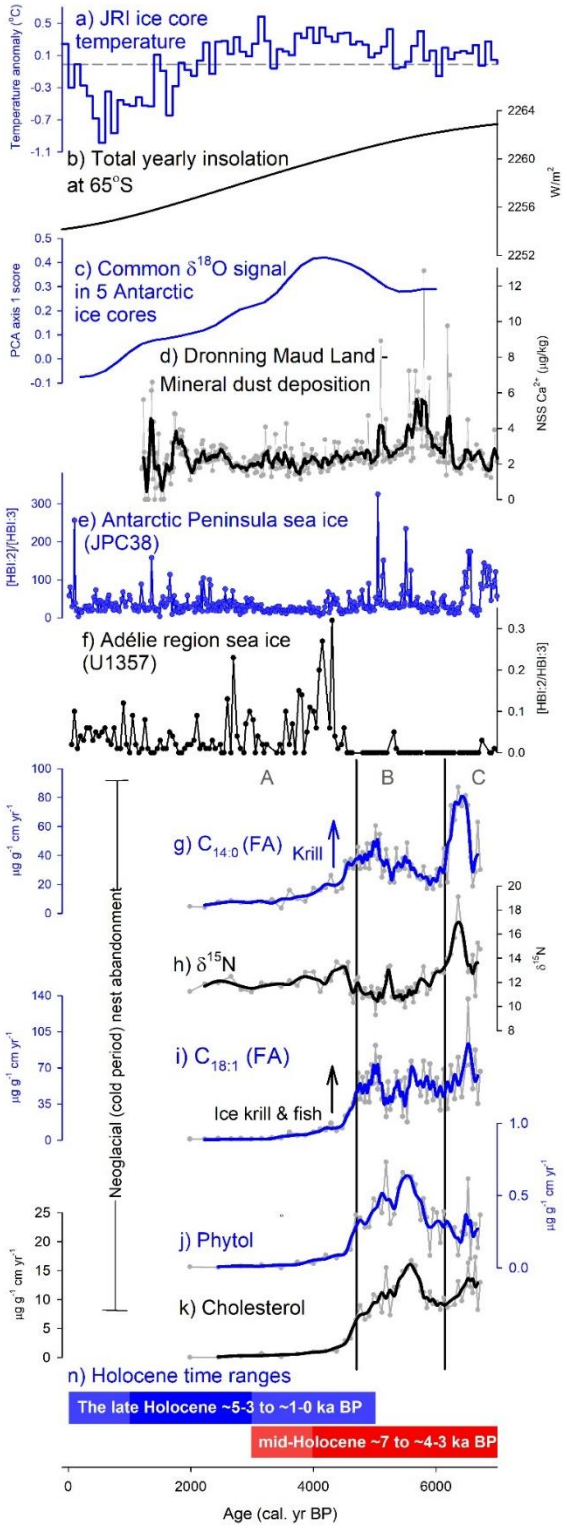

https://doi.org/10.5194/egusphere-2025-513
Preprint. Discussion started: 25 February 2025

Figure 6: Summary plot comparing the marine and ice-core climate proxies (a-f) with 3012MUM2 geochemical proxy data (g – k). (a) James Ross Island (JRI) ice core temperature anomaly relative to 1961-1990 mean based on 100-year averages in Mulvaney et al. (2012); (b) Total yearly insolation at 65°S (Laskar et al., 2004); (c) Common $\delta^{18}O$ signal in 5 Antarctic ice cores, interpreted by PCA axis 1 scores from Hodgson and Bentley (2013) based on common and residual signals in five Antarctic $\delta^{18}O$ records; Vostok, Taylor Dome, EPICA Dome C, EPICA Dronning Maud Land and Dome Fuji (Masson-Delmotte et al., 2011); (d) Dronning Maud Land mineral dust deposition from NSS (non-sea salt) Ca^{2+} from the EPICA DML (EDML) ice core (Fischer et al., 2007); (e) Antarctic Peninsula sea ice from the ratio of highly-branched isoprenoid (HBI) diene to triene (core JPC38) (Barbara et al., 2016); (f) Adélie region sea ice from the ratio of HBI diene to triene (core U1257) (Ashley et al., 2021); (g) $C_{14:0}$ (FA) flux as a krill maker; (h) nitrogen stable isotopes ($\delta^{15}N$); (i) $C_{18:1}$ (FA) as an ice krill and fish marker; (j) phytol flux as a productivity marker; (k) cholesterol flux; and (n) Holocene time ranges for palaeoclimate periods from Crosta et al. (2022). Smooth lines are calculated from appropriate moving averages. Cluster boundaries are based in organic zones A-C in Fig.3.

4.4 Reconstructing ocean productivity using snow-petrel stomach oil markers

For the first time we find significant utility in stomach oil phytol and cholesterol as markers of ocean productivity and diet (Fig. 3 & 6). Phytol is formed from chlorophyll-*a* (Rontani and Volkman, 2003) and is brought into snow petrel diet through krill gut contents (Sargent and Falk-Petersen, 1981). Cholesterol is ubiquitous in living matter but is especially high in krill (Ju and Harvey, 2004), and lower in fish. In the stomach oil record the phytol record is highest in the gradual transition ice organic zone B, indicating access to phytoplankton-rich foraging grounds (greater than in the warmest period e.g. organic zone C) both in the open ocean type configuration and within coastal polynyas scenarios (Fig. 5) close to ice shelves which were in a retreating phase prior to/around this time (Grieman et al., 2024). In organic zone B high nitrogen-containing pigments may have contributed to elevated nitrogen levels. It is also likely that during this period of high accumulation rate (organic zone B) there may also have been enhanced preservation of N containing compounds.

Importantly, cholesterol is highest in zone organic C, a period which we interpret from fatty acid signatures to have had highest dietary abundances of both fish and krill. Phytol and cholesterol likely reflect evidence of high-productivity krill-rich polynyas (coastal or open ocean types). Here we interpret high productivity (evidenced by high phytol) as an expression of the ice shelf front polynya moving south through the foraging range (see zone organic C). The retreating ice edge with associated coastal polynyas could also potentially lead to more frequent occupation of the nest site and concomitant high stomach oil accumulation.

4.5 Isotopic shifts coherent with mid-Holocene warming, increased productivity and potential opening of the Maud Rise polynya

The combination of elevated $\delta^{15}N$ and fatty acid concentrations in the early part of the record may reflect an opening of the Maud Rise polynya which forms intermittently above Maud Rise plateau (Fig. 1) (Jena and Pillai, 2020; Turner et al., 2020; Holland, 2001). High contributions of Antarctic krill in organic zone C (e.g. peak $C_{14:0}$ FA fluxes ~6400 cal. yr BP) are coincident with a high $\delta^{15}N$ (~ 20 ‰) (Fig. 3). The $\delta^{15}N$ values are exceptionally high, exceeding those observed in modern southern ocean top predators (~12–14 ‰) (Hückstädt et al., 2012; Valenzuela et al., 2018; Reisinger et al., 2016; Van Den Berg et al., 2021). The increase in $\delta^{15}N$ is unlikely to reflect high trophic status, because the high Antarctic krill contributions would be expected to introduce lower $\delta^{15}N$ than fish (Rau et al., 1992). Nor can a shift towards coastal foraging, where $\delta^{15}N$

https://doi.org/10.5194/egusphere-2025-513
Preprint. Discussion started: 25 February 2025

values are high (St John Glew et al., 2021), offer an explanation, because the fatty acid markers clearly indicate a mixed diet requiring contributions from both fish and krill (Fig. 3). Instead, we suggest that a baseline shift in $\delta^{15}N$ occurred, whereby enhanced nutrient delivery was facilitated by upwelling, potentially of circumpolar deep water (CDW). In turn, elevated productivity would have been stimulated, evidenced by the high phytol fluxes at this time.

We argue that the high krill consumption is probably linked to the enhanced opening of the large open-ocean Maud Rise polynya, which we posit may give space for early productivity, due to more ice free environments when solar radiation starts to increase in the austral spring (e.g. (Goosse et al., 2021; Jena et al., 2019; Von Berg et al., 2020)). Changes in wind activity may also play a role in Maud Rise polynya formation, much as it does today (Zhou et al., 2022; Francis et al., 2019). Opening of polynyas typically lead to higher productivity and the potential for higher krill (Kang et al., 2020; La et al., 2015). A palaeoreconstruction over the past ~700 years from the sub-Antarctic Marion Island highlight how during cooler periods (e.g. Little Ice Age), winds weakened moving towards the equator, but during warm periods they increased and transitioned towards the pole (Perren et al., 2020). Therefore, it seems feasible that latitudinal shifts in the core wind belt over the Holocene could contribute to changes in the Maud Rise polynya, helping to explain shifts between organic zones (Fig. 3 & 5).

4.6 Synchrony between the north west Weddell Sea sea ice stomach-oil record and Southern Hemisphere palaeoclimate records

There are wider similarities between our Weddell Sea sea ice record and proxy records from the continental ice sheet, from Southern Ocean sediments, and in coastal sediments the opposite side of Antarctica, off Adélie Land, pointing to broader earth-system changes over the Holocene (e.g. insolation forcing, oceanographic and ice sheet changes) (Fig. 6).

Broader changes in stomach oil deposit 3012MUM2, which point to a more productive organic zone C and part of organic zone B compared with a less productive organic zone A identify the widely recognised hypsithermal to neoglacial transition [e.g. (Crosta et al., 2022)]. Changes between the two periods are congruous with an early and productive mid-Holocene warming (also referred to as the Hypsithermal; (Bentley et al., 2009). Climate warming was broadly consistent with ice loss in parts of the Antarctic Peninsula (Johnson et al., 2019; Totten et al., 2015; Michalchuk et al., 2009; Majewski and Anderson, 2009) and completion of the retreat of Filchner and Ronne Ice Shelf (Hillenbrand et al., 2014). The general mid-Holocene warming to neoglacial transition is also consistent with James Ross Island (JRI) ice core temperature in the northwestern Weddell Sea (Mulvaney et al., 2012) which begins to decline from its highest point ~3100 yr BP (Fig. 6). It is further consistent with the broader decreasing $\delta^{18}O$ signal in 5 Antarctic ice cores, interpreted by PCA axis 1 scores based on common and residual signals in $\delta^{18}O$ records (Hodgson and Bentley, 2013; Masson-Delmotte et al., 2011) (Fig. 6). Remarkably, high non-sea salt deposition (Ca^{2+}) from ice cores taken in Dronning Maud Land reflecting wind-blown dust – predominantly from Patagonia (Fischer et al., 2007) is broadly in line with the period of high phytol (indicating high primary productivity) (Fig. 6). An exact causal mechanism between the two records is uncertain as dust is unlikely to be sufficient to stimulate algae at the oceanographic scale at Holocene timescales, even though it can at glacial timescales (Martínez-Garcia et al., 2009; Martínez-Garcia et al., 2011). However even slight changes in wind patterns and intensity can also affect sea ice

https://doi.org/10.5194/egusphere-2025-513
Preprint. Discussion started: 25 February 2025

cover which we purport to be a more likely potential driver typically linked to stratification and iron imitation [e.g. (Sigman et al., 2004; Martínez-Garcia et al., 2009)] and enable both deposition of dust on Antarctica while also influencing decadal-scale sea ice cover.

Sea ice cover also shows wider southern hemispheric patterns. Off the Antarctic Peninsula (JPC38 – South Eastern tip) there was a slightly higher ratio of sea-ice dwelling diatoms (HBI diene) compared with pelagic diatoms (HBI triene) in organic zones B and C of deposit 3012MUM2, compared with the more 'neoglacial' cooler organic zone A (Barbara et al., 2016) (Fig. 6). The HBI ratio is complex as environments with high HBI diene (intermediate presence of sea ice (Belt et al., 2016)) are likely to be ideal environments for snow petrel feeding given their close affinity to sea ice (Delord et al., 2016; Ainley and Jacobs, 1981; Ainley et al., 2017), providing confidence that the neighbouring Weddell Sea was likely to have been a good environment for feeding, consistent with the productive and rich deposit at this time. However, remarkably the transition around ~4700 cal. yr BP to cooler, neoglacial conditions in deposit 3012MUM2 is contemporaneous with a distinct switch to more sea ice in the distant Adélie region at the opposite side of Antarctica, inferred by HBI ratios in core U1357 (Ashley et al., 2021) (Fig. 6F). Ashley et al. (2021) suggest that although the mechanistic driver is not fully resolved, a potential explanation could be the retreat of grounded ice, development of large ice shelf cavities and subsequent altering of AABW and AASW (Antarctic Surface Water). The wider timing of this key transition evidenced in 3012MUM2 ~4700 cal. yr BP could point to a similar mechanism in the Weddell Sea, linked to "ice-pump" enhancement of sub-ice shelf circulation, facilitating the non-linear transition observed (Ashley et al., 2021).

Remarkably the key shift (evidenced between organic zones A & B, ~4700) in the stomach oil deposit is also in phase with a marked transition seen in South Atlantic cores (Hodell et al., 2001) where IRD (as % lithics) increase markedly from ~5 ka BP suggesting cooling waters (together with concomitant changes in diatoms SST index and $\delta^{18}O$ on diatoms) which have been linked to the arrival of more sea ice from the Weddell Sea region (core TTN057-13-PC4). Hodell et al. (2001) highlight the wider similarities with non-linear responses in gradual changes in the Northern Hemisphere, coinciding with rapid changes in middle Holocene climate evidenced from Taylor Dome ice core (Steig et al., 1998). This sediment core record highlights the switch between the mid-Holocene warming and the beginning of neoglacial in the mid Holocene (Hodell et al., 2001). Divine et al. (2010) highlight similar transitions in more cores (also TN057-17-PC1 & TN057-13-PC4) in the Southern Ocean pointing to a clear neoglacial after ~4000 yr BP associated with strengthening of the westerlies and cooling in the inland ice sheet. Hodell et al. (2001) suggest a wider mechanism - although as yet unconfirmed - could be broadly related to insolation changes generating complex feedback at different latitudes of the Southern Ocean and Northern Hemisphere. In terms of insolation, although the Southern Ocean broadly saw an increase in summer insolation from the start of the record, total yearly insolation (e.g. at 65°S) features a decline, providing evidence of an overarching mechanism which may contribute to the mid-Holocene warming to neoglacial transition (Fig. 6). However, modelling suggests that insolation is unlikely to be the sole driver of the transition (Divine et al., 2010; Renssen et al., 2005): variations in sea ice extent in the Southern Ocean are suggested to be a more important driver (Knorr and Lohmann, 2003). The convincing detailed responses in productivity,

https://doi.org/10.5194/egusphere-2025-513
Preprint. Discussion started: 25 February 2025

accumulation, and dietary source markers in deposit 3012MUM2 [e.g. accumulation rates of cholesterol, phytol and fatty acids (Fig. 6)] highlight the role of regional oceanographic and sea-ice dominated forcings.

5 Conclusions

Analyses of accumulation rates and a range of biomarkers in a snow petrel stomach-oil deposit from the Heimefrontfjella Range have been used to infer sea ice and climate in the northeastern Weddell Sea over the Holocene. The record broadly follows a three-zone Holocene climate evolution consistent with changes recorded in the northwestern Weddell Sea and wider regional patterns seen in Antarctica and the Southern Ocean (Crosta et al., 2022). In the first stage between 6700–6200 cal. yr BP high stomach oil accumulation rates and high concentrations of both fish and krill fatty acids suggest easy access to productive foraging grounds. This is consistent with low sea ice cover and extensive polynyas associated with warmer temperatures and regional ice shelf retreat. In the second stage, between 6200–4700 cal. yr BP reductions in accumulation rates of both Antarctic krill fatty acids (e.g. $C_{14:0}$) and fatty acids mainly from fish (e.g. $C_{18:0}$) are used to infer a gradual transition to a more extensive sea-ice configuration restricting access to pelagic foraging grounds. This is consistent with a switch towards foraging in coastal polynyas at the ice-shelf front. In the third stage, between 4600 and 2000 cal. yr BP low stomach oil accumulation rates and reductions in fatty acid and productivity markers indicate that increased sea ice extent restricted access to foraging grounds and by ~6700 cal. yr BP resulted in abandonment of the nest site. This is consistent with the transition to cooler neoglacial conditions seen in a range of records from the northwestern Weddell Sea (Barbara et al., 2016; Nie et al., 2022), from ice records on the Antarctic continent (Hodgson and Bentley, 2013), and changes elsewhere in the wider Antarctic region including Adélie Land (Ashley et al., 2021) and the South Atlantic (Hodell et al., 2001; Divine et al., 2010). This study has also shown, for the first time, the utility of phytol and cholesterol for tracking past snow petrel diet and thus interpretation of environmental conditions.

Data availability

All data presented within this manuscript has been submitted to data repository PANGAEA (PDI-40423)

Author contributions

ELM obtained main funding. MAS, DRG, NT, CL, AG & ELM carried out the laboratory work and data analysis. MJB & DAH collected samples from Antarctica. MAS prepared the initial paper, discussing initial primary interpretations with ELM, MJB & DAH.

https://doi.org/10.5194/egusphere-2025-513
Preprint. Discussion started: 25 February 2025

Competing interests

Some authors are members of the editorial board of the journal Climate of the Past. The authors also have no other competing interests to declare.

Acknowledgements

We thank the BAS field operations staff and pilots who supported the work along with Andy Hein and Al Davies who helped with sampling. We thank Kerry A. Strong, Martin D. West and Amanda Hayton for laboratory assistance. We also thank Helen Mackay for advice and assistance regarding the interpretation of sterols and stanols. We thank Ewan Wakefield for insights on snow petrel feeding ranges and seasonality, plus James Grecian for discussion of Southern Ocean/Weddell Sea species distribution references. We also thank Chris Orton for drafting Figure 5.

Financial support

This research was supported by the European Research Council H2020 (ANTSIE (grant no. 864637)) and the Leverhulme Trust (Philip Leverhulme Research Leadership Award, RL-2019-023). Deposit 3012MUM2 was collected as part of a NERC-funded award to MB and DH on past ice sheet and environmental change in Coats Land (Reference: NE/K003674/1).

References

Ainley, D., Woehler, E. J., and Lescroël, A. Birds and Antarctic sea ice, in: Sea Ice 570-582 doi: 10.1002/9781118778371, 2017.

Ainley, D. G. and Jacobs, S. S. Sea-bird affinities for ocean and ice boundaries in the Antarctic *Deep Sea Research Part A. Oceanographic Research Papers* 28 1173-1185, 1981.

Ainley, D. G., O'Connor, E. F., and Boekelheide, R. J. The Marine Ecology of Birds in the Ross Sea, Antarctica *Ornithological Monographs* iii-97, 1984.

Ainley, D. G., Jacobs, S. S., Ribic, C. A., and Gaffney, I. Seabird distribution and oceanic features of the Amundsen and southern Bellingshausen seas *Antarctic Science* 10 111-123, 1998.

Ainley, D. G., Hobson, K. A., Crosta, X., Rau, G. H., Wassenaar, L. I., and Augustinus, P. C. Holocene variation in the Antarctic coastal food web: linking δD and $\delta^{13}C$ in snow petrel diet and marine sediments *Mar. Ecol. Prog. Ser.* 306 31-40, 2006.

Ashley, K. E., McKay, R., Etourneau, J., Jimenez-Espejo, F. J., Condron, A., Albot, A., Crosta, X., Riesselman, C., Seki, O., Massé, G., Golledge, N. R., Gasson, E., Lowry, D. P., Barrand, N. E., Johnson, K., Bertler, N., Escutia, C., Dunbar, R., and Bendle, J. A. Mid-Holocene Antarctic sea-ice increase driven by marine ice sheet retreat *Clim. Past* 17 1-19, 2021.

Bak, Y.-S., Yoo, K.-C., Yoon, H. I., Lee, J.-D., and Yun, H. Diatom evidence for Holocene paleoclimatic change in the South Scotia Sea, West Antarctica *Geosciences Journal* 11 11-22, 2007.

Barbara, L., Crosta, X., Massé, G., and Ther, O. Deglacial environments in eastern Prydz Bay, East Antarctica *Quaternary Science Reviews* 29 2731-2740, 2010.

Barbara, L., Crosta, X., Schmidt, S., and Massé, G. Diatoms and biomarkers evidence for major changes in sea ice conditions prior the instrumental period in Antarctic Peninsula *Quaternary Science Reviews* 79 99-110, 2013.

https://doi.org/10.5194/egusphere-2025-513
Preprint. Discussion started: 25 February 2025

Barbara, L., Crosta, X., Leventer, A., Schmidt, S., Etourneau, J., Domack, E., and Massé, G. Environmental responses of the Northeast Antarctic Peninsula to the Holocene climate variability *Paleoceanography* 31 131-147, 2016.

Belt, S. T., Smik, L., Brown, T. A., Kim, J.-H., Rowland, S. J., Allen, C. S., Gal, J.-K., Shin, K.-H., Lee, J. I., and Taylor, K. W. Source identification and distribution reveals the potential of the geochemical Antarctic sea ice proxy $IPSO_{25}$ *Nature Communications* 7 1-10, 2016.

Bennett, K. D. Determination of the number of zones in a biostratigraphical sequence *New Phytologist* 132 155-170, 1996.

Bentley, M. J., Hodgson, D. A., Smith, J. A., Cofaigh, C. Ó., Domack, E. W., Larter, R. D., Roberts, S. J., Brachfeld, S., Leventer, A., Hjort, C., Hillenbrand, C.-D., and Evans, J. Mechanisms of Holocene palaeoenvironmental change in the Antarctic Peninsula region *The Holocene* 19 51-69, 2009.

Bentley, M. J., Ó Cofaigh, C., Anderson, J. B., Conway, H., Davies, B., Graham, A. G. C., Hillenbrand, C.-D., Hodgson, D. A., Jamieson, S. S. R., Larter, R. D., Mackintosh, A., Smith, J. A., Verleyen, E., Ackert, R. P., Bart, P. J., Berg, S., Brunstein, D., Canals, M., Colhoun, E. A., Crosta, X., Dickens, W. A., Domack, E., Dowdeswell, J. A., Dunbar, R., Ehrmann, W., Evans, J., Favier, V., Fink, D., Fogwill, C. J., Glasser, N. F., Gohl, K., Golledge, N. R., Goodwin, I., Gore, D. B., Greenwood, S. L., Hall, B. L., Hall, K., Hedding, D. W., Hein, A. S., Hocking, E. P., Jakobsson, M., Johnson, J. S., Jomelli, V., Jones, R. S., Klages, J. P., Kristoffersen, Y., Kuhn, G., Leventer, A., Licht, K., Lilly, K., Lindow, J., Livingstone, S. J., Massé, G., McGlone, M. S., McKay, R. M., Melles, M., Miura, H., Mulvaney, R., Nel, W., Nitsche, F. O., O'Brien, P. E., Post, A. L., Roberts, S. J., Saunders, K. M., Selkirk, P. M., Simms, A. R., Spiegel, C., Stolldorf, T. D., Sugden, D. E., van der Putten, N., van Ommen, T., Verfaillie, D., Vyverman, W., Wagner, B., White, D. A., Witus, A. E., and Zwartz, D. A community-based geological reconstruction of Antarctic Ice Sheet deglaciation since the Last Glacial Maximum *Quaternary Science Reviews* 100 1-9, 2014.

Berg, S., Melles, M., Hermichen, W.-D., McClymont, E. L., Bentley, M. J., Hodgson, D. A., and Kuhn, G. Evaluation of Mumiyo Deposits From East Antarctica as Archives for the Late Quaternary Environmental and Climatic History *Geochemistry, Geophysics, Geosystems* 20 260-276, 2019.

Berg, S., Emmerson, L., Heim, C., Buchta, E., Fromm, T., Glaser, B., Hermichen, W.-D., Rethemeyer, J., Southwell, C., Wand, U., Zech, M., and Melles, M. Reconstructing the Paleo-Ecological Diet of Snow Petrels (Pagodroma nivea) From Modern Samples and Fossil Deposits: Implications for Southern Ocean Paleoenvironmental Reconstructions *Journal of Geophysical Research: Biogeosciences* 128 e2023JG007454, 2023.

Björck, S., Hjort, C., Ingólfsson, O., and Skog, G Radiocarbon dates from the Antarctic Peninsula – problems and potential, in: Radiocarbon Dating: Recent Applications and Future Potential edited by: Lowe, J. J. Quaternary Research Association Cambridge 55-65, 1991a.

Björck, S. H., C. Ingófsson, O. Skog, G.: Radiocarbon dates from the Antarctic Peninsula problems and potential, Radiocarbon Dating: Recent Applications and Future Potential. Quat. Proc., 1, Cambridge, 55-56, 1991b.

Blaauw, M. and Christen, J. A. Flexible paleoclimate age-depth models using an autoregressive gamma process *Bayesian Anal.* 6 457-474, 2011.

Blaauw, M., Christen, J. A., Lopez, M. A. A., Vazquez, J. E., Belding, T., Theiler, J., Gough, B., Karney, C., Rcpp, L., and Blaauw, M. M. Package 'rbacon' 2023.

Brandon, M. A., Cottier, F. R., and Nilsen, F. Sea Ice and Oceanography, in: Sea Ice 2nd Edition ed. edited by: Thomas, D. N., and Dieckmann, G., S. Wiley-Blackwell Chichester, United Kingdom 79-111, 2010.

Bridges, C. Structure and function of krill (Euphasia superba) hemocyanin-adaption to life at low temperature *Structure and function of invertebrate respiratory proteins Life Chemistry Reports* 1 353-356, 1983.

Castro, M. F., Neves, J. C. L., Francelino, M. R., Schaefer, C. E. G. R., and Oliveira, T. S. Seabirds enrich Antarctic soil with trace metals in organic fractions *Science of The Total Environment* 785 147271, 2021.

Cheng, W., Sun, L., Kimpe, L. E., Mallory, M. L., Smol, J. P., Gallant, L. R., Li, J., and Blais, J. M. Sterols and Stanols Preserved in Pond Sediments Track Seabird Biovectors in a High Arctic Environment *Environmental Science & Technology* 50 9351-9360, 2016.

Collins, M., Knutti, R., Arblaster, J., Dufresne, J.-L., Fichefet, T., Friedlingstein, P., Gao, X., Gutowski, W. J., Johns, T., and Krinner, G. Long-term climate change: projections, commitments and irreversibility, in: Climate Change 2013-The Physical Science Basis: Contribution of Working Group I to the Fifth Assessment Report of the Intergovernmental Panel on Climate Change Cambridge University Press 1029-1136, 2013.

Comiso, J. C. and Gordon, A. L. Recurring polynyas over the Cosmonaut Sea and the Maud Rise *Journal of Geophysical Research: Oceans* 92 2819-2833, 1987.

https://doi.org/10.5194/egusphere-2025-513
Preprint. Discussion started: 25 February 2025

Cripps, G. C., Watkins, J. L., Hill, H. J., and Atkinson, A. Fatty acid content of Antarctic krill Euphausia superba at South Georgia related to regional populations and variations in diet *Mar. Ecol. Prog. Ser.* 181 177-188, 1999.

Crosta, X., Kohfeld, K. E., Bostock, H. C., Chadwick, M., Du Vivier, A., Esper, O., Etourneau, J., Jones, J., Leventer, A., Müller, J., Rhodes, R. H., Allen, C. S., Ghadi, P., Lamping, N., Lange, C. B., Lawler, K. A., Lund, D., Marzocchi, A., Meissner, K. J., Menviel, L., Nair, A., Patterson, M., Pike, J., Prebble, J. G., Riesselman, C., Sadatzki, H., Sime, L. C., Shukla, S. K., Thöle, L., Vorrath, M. E., Xiao, W., and Yang, J. Antarctic sea ice over the past 130 000 years – Part 1: a review of what proxy records tell us *Clim. Past* 18 1729-1756, 2022.

Delord, K., Pinet, P., Pinaud, D., Barbraud, C., De Grissac, S., Lewden, A., Cherel, Y., and Weimerskirch, H. Species-specific foraging strategies and segregation mechanisms of sympatric Antarctic fulmarine petrels throughout the annual cycle *Ibis* 158 569-586, 2016.

Denis, D., Crosta, X., Barbara, L., Massé, G., Renssen, H., Ther, O., and Giraudeau, J. Sea ice and wind variability during the Holocene in East Antarctica: insight on middle–high latitude coupling *Quaternary Science Reviews* 29 3709-3719, 2010.

Divine, D. V., Koç, N., Isaksson, E., Nielsen, S., Crosta, X., and Godtliebsen, F. Holocene Antarctic climate variability from ice and marine sediment cores: Insights on ocean–atmosphere interaction *Quaternary Science Reviews* 29 303-312, 2010.

Eayrs, C., Li, X., Raphael, M. N., and Holland, D. M. Rapid decline in Antarctic sea ice in recent years hints at future change *Nature Geoscience* 14 460-464, 2021.

Etourneau, J., Collins, L. G., Willmott, V., Kim, J. H., Barbara, L., Leventer, A., Schouten, S., Sinninghe Damsté, J. S., Bianchini, A., Klein, V., Crosta, X., and Massé, G. Holocene climate variations in the western Antarctic Peninsula: evidence for sea ice extent predominantly controlled by changes in insolation and ENSO variability *Clim. Past* 9 1431-1446, 2013.

Ferrari, R., Jansen, M. F., Adkins, J. F., Burke, A., Stewart, A. L., and Thompson, A. F. Antarctic sea ice control on ocean circulation in present and glacial climates *Proceedings of the National Academy of Sciences* 111 8753-8758, 2014.

Fetterer, F., Knowles, K., Meier, W., Savoie, M., and Windnagel, A.: Updated daily. Sea Ice Index, Version 3, Boulder, Colorado USA. NSIDC: National Snow and Ice Data Center, 10.7265/N5K072F8, 2017.

Fischer, H., Fundel, F., Ruth, U., Twarloh, B., Wegner, A., Udisti, R., Becagli, S., Castellano, E., Morganti, A., Severi, M., Wolff, E., Littot, G., Röthlisberger, R., Mulvaney, R., Hutterli, M. A., Kaufmann, P., Federer, U., Lambert, F., Bigler, M., Hansson, M., Jonsell, U., de Angelis, M., Boutron, C., Siggaard-Andersen, M.-L., Steffensen, J. P., Barbante, C., Gaspari, V., Gabrielli, P., and Wagenbach, D. Reconstruction of millennial changes in dust emission, transport and regional sea ice coverage using the deep EPICA ice cores from the Atlantic and Indian Ocean sector of Antarctica *Earth and Planetary Science Letters* 260 340-354, 2007.

Francis, D., Eayrs, C., Cuesta, J., and Holland, D. Polar Cyclones at the Origin of the Reoccurrence of the Maud Rise Polynya in Austral Winter 2017 *Journal of Geophysical Research: Atmospheres* 124 5251-5267, 2019.

Freer, J. J., Tarling, G. A., Collins, M. A., Partridge, J. C., and Genner, M. J. Predicting future distributions of lanternfish, a significant ecological resource within the Southern Ocean *Diversity and Distributions* 25 1259-1272, 2019.

Gilbert, E. and Holmes, C. 2023's Antarctic sea ice extent is the lowest on record *Weather* 79 46-51, 2024.

Goosse, H., Dalaiden, Q., Cavitte, M. G. P., and Zhang, L. Can we reconstruct the formation of large open-ocean polynyas in the Southern Ocean using ice core records? *Clim. Past* 17 111-131, 2021.

Grieman, M. M., Nehrbass-Ahles, C., Hoffmann, H. M., Bauska, T. K., King, A. C. F., Mulvaney, R., Rhodes, R. H., Rowell, I. F., Thomas, E. R., and Wolff, E. W. Abrupt Holocene ice loss due to thinning and ungrounding in the Weddell Sea Embayment *Nature Geoscience* 17 227-232, 2024.

Heaton, T. J., Köhler, P., Butzin, M., Bard, E., Reimer, R. W., Austin, W. E. N., Bronk Ramsey, C., Grootes, P. M., Hughen, K. A., Kromer, B., Reimer, P. J., Adkins, J., Burke, A., Cook, M. S., Olsen, J., and Skinner, L. C. Marine20—The Marine Radiocarbon Age Calibration Curve (0–55,000 cal BP) *Radiocarbon* 62 779-820, 2020.

Hillenbrand, C.-D., Bentley, M. J., Stolldorf, T. D., Hein, A. S., Kuhn, G., Graham, A. G. C., Fogwill, C. J., Kristoffersen, Y., Smith, J. A., Anderson, J. B., Larter, R. D., Melles, M., Hodgson, D. A., Mulvaney, R., and Sugden, D. E. Reconstruction of changes in the Weddell Sea sector of the Antarctic Ice Sheet since the Last Glacial Maximum *Quaternary Science Reviews* 100 111-136, 2014.

Hillenbrand, C.-D., Smith, J. A., Hodell, D. A., Greaves, M., Poole, C. R., Kender, S., Williams, M., Andersen, T. J., Jernas, P. E., Elderfield, H., Klages, J. P., Roberts, S. J., Gohl, K., Larter, R. D., and Kuhn, G. West Antarctic Ice Sheet retreat driven by Holocene warm water incursions *Nature* 547 43-48, 2017.

https://doi.org/10.5194/egusphere-2025-513
Preprint. Discussion started: 25 February 2025

Hiller, A., Wand, U., Kämpf, H., and Stackebrandt, W. Occupation of the Antarctic continent by petrels during the past 35 000 years: Inferences from a 14C study of stomach oil deposits *Polar Biology* 9 69-77, 1988.

Hodell, D. A., Kanfoush, S. L., Shemesh, A., Crosta, X., Charles, C. D., and Guilderson, T. P. Abrupt Cooling of Antarctic Surface Waters and Sea Ice Expansion in the South Atlantic Sector of the Southern Ocean at 5000 cal yr B.P *Quaternary Research* 56 191-198, 2001.

Hodgson, D. A. and Bentley, M. J. Lake highstands in the Pensacola Mountains and Shackleton Range 4300–2250 cal. yr BP: Evidence of a warm climate anomaly in the interior of Antarctica *The Holocene* 23 388-397, 2013.

Hodgson, D. A., Hogan, K., Smith, J. M., Smith, J. A., Hillenbrand, C. D., Graham, A. G. C., Fretwell, P., Allen, C., Peck, V., Arndt, J. E., Dorschel, B., Hübscher, C., Smith, A. M., and Larter, R. Deglaciation and future stability of the Coats Land ice margin, Antarctica *The Cryosphere* 12 2383-2399, 2018.

Holland, D. M. Explaining the Weddell Polynya--a Large Ocean Eddy Shed at Maud Rise *Science* 292 1697-1700, 2001.

Hückstädt, L. A., Koch, P. L., McDonald, B. I., Goebel, M. E., Crocker, D. E., and Costa, D. P. Stable isotope analyses reveal individual variability in the trophic ecology of a top marine predator, the southern elephant seal *Oecologia* 169 395-406, 2012.

Hughes, C., Johnson, M., von Glasow, R., Chance, R., Atkinson, H., Souster, T., Lee, G. A., Clarke, A., Meredith, M., Venables, H. J., Turner, S. M., Malin, G., and Liss, P. S. Climate-induced change in biogenic bromine emissions from the Antarctic marine biosphere *Global Biogeochemical Cycles* 26 2012.

Imber, M. J. The Origin of Petrel Stomach Oils: A Review *The Condor* 78 366-369, 1976.

Ionita, M. Large-scale drivers of the exceptionally low winter Antarctic sea ice extent in 2023 *Frontiers in Earth Science* 12 2024.

Jena, B. and Pillai, A. N. Satellite observations of unprecedented phytoplankton blooms in the Maud Rise polynya, Southern Ocean *The Cryosphere* 14 1385-1398, 2020.

Jena, B., Ravichandran, M., and Turner, J. Recent Reoccurrence of Large Open-Ocean Polynya on the Maud Rise Seamount *Geophysical Research Letters* 46 4320-4329, 2019.

Johnson, J. S., Nichols, K. A., Goehring, B. M., Balco, G., and Schaefer, J. M. Abrupt mid-Holocene ice loss in the western Weddell Sea Embayment of Antarctica *Earth and Planetary Science Letters* 518 127-135, 2019.

Ju, S.-J. and Harvey, H. R. Lipids as markers of nutritional condition and diet in the Antarctic krill Euphausia superba and Euphausia crystallorophias during austral winter *Deep Sea Research Part II: Topical Studies in Oceanography* 51 2199-2214, 2004.

Juggins, S. rioja: Analysis of Quaternary Science Data. R package version 0.9-26 *University of Newcastle, Newcastle upon Tyne* 2020.

Kang, M., Fajaryanti, R., Son, W., Kim, J.-H., and La, H. S. Acoustic Detection of Krill Scattering Layer in the Terra Nova Bay Polynya, Antarctica *Frontiers in Marine Science* 7 2020.

Knorr, G. and Lohmann, G. Southern Ocean origin for the resumption of Atlantic thermohaline circulation during deglaciation *Nature* 424 532-536, 2003.

Kyrmanidou, A., Vadman, K. J., Ishman, S. E., Leventer, A., Brachfeld, S., Domack, E. W., and Wellner, J. S. Late Holocene oceanographic and climatic variability recorded by the Perseverance Drift, northwestern Weddell Sea, based on benthic foraminifera and diatoms *Marine Micropaleontology* 141 10-22, 2018.

La, H. S., Lee, H., Fielding, S., Kang, D., Ha, H. K., Atkinson, A., Park, J., Siegel, V., Lee, S., and Shin, H. C. High density of ice krill (Euphausia crystallorophias) in the Amundsen sea coastal polynya, Antarctica *Deep Sea Research Part I: Oceanographic Research Papers* 95 75-84, 2015.

Laskar, J., Robutel, P., Joutel, F., Gastineau, M., Correia, A. C. M., and Levrard, B. A long-term numerical solution for the insolation quantities of the Earth *A&A* 428 261-285, 2004.

Lewis, R. W. Studies of the glyceryl ethers of the stomach oil of Leach's petrel Oceanodroma leucorhoa (Viellot) *Comparative Biochemistry and Physiology* 19 363-377, 1966.

Lewis, R. W. Studies on the stomach oils of marine animals—II. Oils of some procellariiform birds *Comparative Biochemistry and Physiology* 31 725-731, 1969.

Liu, S., Liu, Y., Teschke, K., Hindell, M. A., Downey, R., Woods, B., Kang, B., Ma, S., Zhang, C., Li, J., Ye, Z., Sun, P., He, J., and Tian, Y. Incorporating mesopelagic fish into the evaluation of conservation areas for marine living resources under climate change scenarios *Marine Life Science & Technology* 6 68-83, 2024.

https://doi.org/10.5194/egusphere-2025-513
Preprint. Discussion started: 25 February 2025

Liu, X., Sun, L., Xie, Z., Yin, X., and Wang, Y. A 1300-year Record of Penguin Populations at Ardley Island in the Antarctic, as Deduced from the Geochemical Data in the Ornithogenic Lake Sediments *Arctic, Antarctic, and Alpine Research* 37 490-498, 2005.

Majewski, W. and Anderson, J. B. Holocene foraminiferal assemblages from Firth of Tay, Antarctic Peninsula: Paleoclimate implications *Marine Micropaleontology* 73 135-147, 2009.

Martínez-Garcia, A., Rosell-Melé, A., Jaccard, S. L., Geibert, W., Sigman, D. M., and Haug, G. H. Southern Ocean dust–climate coupling over the past four million years *Nature* 476 312-315, 2011.

Martínez-Garcia, A., Rosell-Melé, A., Geibert, W., Gersonde, R., Masqué, P., Gaspari, V., and Barbante, C. Links between iron supply, marine productivity, sea surface temperature, and CO2 over the last 1.1 Ma *Paleoceanography* 24 2009.

Masson-Delmotte, V., Buiron, D., Ekaykin, A., Frezzotti, M., Gallée, H., Jouzel, J., Krinner, G., Landais, A., Motoyama, H., Oerter, H., Pol, K., Pollard, D., Ritz, C., Schlosser, E., Sime, L. C., Sodemann, H., Stenni, B., Uemura, R., and Vimeux, F. A comparison of the present and last interglacial periods in six Antarctic ice cores *Clim. Past* 7 397-423, 2011.

McBride, M. M., Schram Stokke, O., Renner, A. H. H., Krafft, B. A., Bergstad, O. A., Biuw, M., Lowther, A. D., and Stiansen, J. E. Antarctic krill Euphausia superba: spatial distribution, abundance, and management of fisheries in a changing climate *Marine Ecology Progress Series* 668 185-214, 2021.

McClymont, E. L., Bentley, M. J., Hodgson, D. A., Spencer-Jones, C. L., Wardley, T., West, M. D., Croudace, I. W., Berg, S., Gröcke, D. R., Kuhn, G., Jamieson, S. S. R., Sime, L., and Phillips, R. A. Summer sea-ice variability on the Antarctic margin during the last glacial period reconstructed from snow petrel (Pagodroma nivea) stomach-oil deposits *Clim. Past* 18 381-403, 2022.

Michalchuk, B. R., Anderson, J. B., Wellner, J. S., Manley, P. L., Majewski, W., and Bohaty, S. Holocene climate and glacial history of the northeastern Antarctic Peninsula: the marine sedimentary record from a long SHALDRIL core *Quaternary Science Reviews* 28 3049-3065, 2009.

Mulvaney, R., Abram, N. J., Hindmarsh, R. C. A., Arrowsmith, C., Fleet, L., Triest, J., Sime, L. C., Alemany, O., and Foord, S. Recent Antarctic Peninsula warming relative to Holocene climate and ice-shelf history *Nature* 489 141-144, 2012.

Nichols, K. A., Goehring, B. M., Balco, G., Johnson, J. S., Hein, A. S., and Todd, C. New Last Glacial Maximum ice thickness constraints for the Weddell Sea Embayment, Antarctica *The Cryosphere* 13 2935-2951, 2019.

Nie, S., Xiao, W., and Wang, R. Mid-Late Holocene climate variabilities in the Bransfield Strait, Antarctic Peninsula driven by insolation and ENSO activities *Palaeogeography, Palaeoclimatology, Palaeoecology* 601 111140, 2022.

Nielsen, S. H. H., Hodell, D. A., Kamenov, G., Guilderson, T., and Perfit, M. R. Origin and significance of ice-rafted detritus in the Atlantic sector of the Southern Ocean *Geochemistry, Geophysics, Geosystems* 8 2007.

Antarctic sea ice at near-record-low maximum extent for 2024, last access: 9 October 2024.

Perren, B. B., Hodgson, D. A., Roberts, S. J., Sime, L., Van Nieuwenhuyze, W., Verleyen, E., and Vyverman, W. Southward migration of the Southern Hemisphere westerly winds corresponds with warming climate over centennial timescales *Communications Earth & Environment* 1 58, 2020.

Purich, A. and Doddridge, E. W. Record low Antarctic sea ice coverage indicates a new sea ice state *Communications Earth & Environment* 4 314, 2023.

Ran, Q., Duan, M., Wang, P., Ye, Z., Mou, J., Wang, X., Tian, Y., Zhang, C., Qiao, H., and Zhang, J. Predicting the current habitat suitability and future habitat changes of Antarctic jonasfish Notolepis coatsorum in the Southern Ocean *Deep Sea Research Part II: Topical Studies in Oceanography* 199 105077, 2022.

Rau, G. H., Ainley, D. G., Bengtson, J. L., Torres, J. J., and Hopkins, T. L. $^{15}N/^{14}N$ and $^{13}C/^{12}C$ in Weddell Sea birds, seals, and fish: implications for diet and trophic structure *Marine Ecology Progress Series* 84 1-8, 1992.

Reisinger, R. R., Gröcke, D. R., Lübcker, N., McClymont, E. L., Hoelzel, A. R., and de Bruyn, P. J. N. Variation in the diet of killer whales Orcinus orca at Marion Island, Southern Ocean *Marine Ecology Progress Series* 549 263-274, 2016.

Renssen, H., Goosse, H., Fichefet, T., Masson-Delmotte, V., and Koç, N. Holocene climate evolution in the high-latitude Southern Hemisphere simulated by a coupled atmosphere-sea ice-ocean-vegetation model *The Holocene* 15 951-964, 2005.

Rignot, E., J. Mouginot, and B. Scheuchl. : MEaSUREs Grounding Zone of the Antarctic Ice Sheet, Version 1. [2018] [dataset], doi: 10.5067/HGLT8XB480E4, 2022.

Roberts, S. J., Monien, P., Foster, L. C., Loftfield, J., Hocking, E. P., Schnetger, B., Pearson, E. J., Juggins, S., Fretwell, P., Ireland, L., Ochyra, R., Haworth, A. R., Allen, C. S., Moreton, S. G., Davies, S. J., Brumsack, H.-J., Bentley, M. J., and

https://doi.org/10.5194/egusphere-2025-513
Preprint. Discussion started: 25 February 2025

Hodgson, D. A. Past penguin colony responses to explosive volcanism on the Antarctic Peninsula *Nature Communications* 8 14914, 2017.
Rontani, J.-F. and Volkman, J. K. Phytol degradation products as biogeochemical tracers in aquatic environments *Organic Geochemistry* 34 1-35, 2003.
Sargent, J. R. and Falk-Petersen, S. Ecological investigations on the zooplankton community in balsfjorden, northern Norway: Lipids and fatty acids in *Meganyctiphanes norvegica*, *Thysanoessa raschi* and *T. inermis* during mid-winter *Mar. Biol.* 62 131-137, 1981.
Sarmiento, J. L., Gruber, N., Brzezinski, M. A., and Dunne, J. P. High-latitude controls of thermocline nutrients and low latitude biological productivity *Nature* 427 56-60, 2004.
Shatova, O., Wing, S. R., Gault-Ringold, M., Wing, L., and Hoffmann, L. J. Seabird guano enhances phytoplankton production in the Southern Ocean *Journal of Experimental Marine Biology and Ecology* 483 74-87, 2016.
Shatova, O. A., Wing, S. R., Hoffmann, L. J., Wing, L. C., and Gault-Ringold, M. Phytoplankton community structure is influenced by seabird guano enrichment in the Southern Ocean *Estuarine, Coastal and Shelf Science* 191 125-135, 2017.
Sigman, D. M., Jaccard, S. L., and Haug, G. H. Polar ocean stratification in a cold climate *Nature* 428 59-63, 2004.
Smith, J. A., Hillenbrand, C.-D., Pudsey, C. J., Allen, C. S., and Graham, A. G. C. The presence of polynyas in the Weddell Sea during the Last Glacial Period with implications for the reconstruction of sea-ice limits and ice sheet history *Earth and Planetary Science Letters* 296 287-298, 2010.
Sparaventi, E., Rodríguez-Romero, A., Barbosa, A., Ramajo, L., and Tovar-Sánchez, A. Trace elements in Antarctic penguins and the potential role of guano as source of recycled metals in the Southern Ocean *Chemosphere* 285 131423, 2021.
St John Glew, K., Espinasse, B., Hunt, B. P. V., Pakhomov, E. A., Bury, S. J., Pinkerton, M., Nodder, S. D., Gutiérrez-Rodríguez, A., Safi, K., Brown, J. C. S., Graham, L., Dunbar, R. B., Mucciarone, D. A., Magozzi, S., Somes, C., and Trueman, C. N. Isoscape Models of the Southern Ocean: Predicting Spatial and Temporal Variability in Carbon and Nitrogen Isotope Compositions of Particulate Organic Matter *Global Biogeochemical Cycles* 35 e2020GB006901, 2021.
Steig, E. J., Hart, C. P., White, J. W. C., Cunningham, W. L., Davis, M. D., and Saltzman, E. S. Changes in climate, ocean and ice-sheet conditions in the Ross embayment, Antarctica, at 6 ka *Annals of Glaciology* 27 305-310, 1998.
Sun, L., Xie, Z., and Zhao, J. A 3,000-year record of penguin populations *Nature* 407 858-858, 2000.
Tatur, A., Myrcha, A., and Niegodzisz, J. Formation of abandoned penguin rookery ecosystems in the maritime Antarctic *Polar Biology* 17 405-417, 1997.
Taylor, F., Whitehead, J., and Domack, E. Holocene paleoclimate change in the Antarctic Peninsula: evidence from the diatom, sedimentary and geochemical record *Mar. Micropaleontol.* 41 25-43, 2001.
Ter Braak, C. and Smilauer, P. Canoco for Windows version 4.5 *Biometris–Plant Research International, Wageningen* 2002.
Totten, R. L., Anderson, J. B., Fernandez, R., and Wellner, J. S. Marine record of Holocene climate, ocean, and cryosphere interactions: Herbert Sound, James Ross Island, Antarctica *Quaternary Science Reviews* 129 239-259, 2015.
Turner, J., Guarino, M. V., Arnatt, J., Jena, B., Marshall, G. J., Phillips, T., Bajish, C. C., Clem, K., Wang, Z., Andersson, T., Murphy, E. J., and Cavanagh, R. Recent Decrease of Summer Sea Ice in the Weddell Sea, Antarctica *Geophysical Research Letters* 47 e2020GL087127, 2020.
Valenzuela, L. O., Rowntree, V. J., Sironi, M., and Seger, J. Stable isotopes ($\delta^{15}N$, $\delta^{13}C$, $\delta^{34}S$) in skin reveal diverse food sources used by southern right whales Eubalaena australis *Marine Ecology Progress Series* 603 243-255, 2018.
van den Berg, G. L., Vermeulen, E., Valenzuela, L. O., Bérubé, M., Ganswindt, A., Gröcke, D. R., Hall, G., Hulva, P., Neveceralova, P., Palsbøll, P. J., and Carroll, E. L. Decadal shift in foraging strategy of a migratory southern ocean predator *Global Change Biology* 27 1052-1067, 2021.
Verleyen, E., Hodgson, D. A., Sabbe, K., Cremer, H., Emslie, S. D., Gibson, J., Hall, B., Imura, S., Kudoh, S., Marshall, G. J., McMinn, A., Melles, M., Newman, L., Roberts, D., Roberts, S. J., Singh, S. M., Sterken, M., Tavernier, I., Verkulich, S., de Vyver, E. V., Van Nieuwenhuyze, W., Wagner, B., and Vyverman, W. Post-glacial regional climate variability along the East Antarctic coastal margin—Evidence from shallow marine and coastal terrestrial records *Earth-Sci. Rev.* 104 199-212, 2011.
Vernet, M., Geibert, W., Hoppema, M., Brown, P. J., Haas, C., Hellmer, H. H., Jokat, W., Jullion, L., Mazloff, M., Bakker, D. C. E., Brearley, J. A., Croot, P., Hattermann, T., Hauck, J., Hillenbrand, C.-D., Hoppe, C. J. M., Huhn, O., Koch, B. P., Lechtenfeld, O. J., Meredith, M. P., Naveira Garabato, A. C., Nöthig, E.-M., Peeken, I., Rutgers van der Loeff, M. M.,

https://doi.org/10.5194/egusphere-2025-513
Preprint. Discussion started: 25 February 2025

Schmidtko, S., Schröder, M., Strass, V. H., Torres-Valdés, S., and Verdy, A. The Weddell Gyre, Southern Ocean: Present Knowledge and Future Challenges *Reviews of Geophysics* 57 623-708, 2019.

von Berg, L., Prend, C. J., Campbell, E. C., Mazloff, M. R., Talley, L. D., and Gille, S. T. Weddell Sea Phytoplankton Blooms Modulated by Sea Ice Variability and Polynya Formation *Geophysical Research Letters* 47 e2020GL087954, 2020.

Wang, J., Massonnet, F., Goosse, H., Luo, H., Barthélemy, A., and Yang, Q. Synergistic atmosphere-ocean-ice influences have driven the 2023 all-time Antarctic sea-ice record low *Communications Earth & Environment* 5 415, 2024.

Warham, J., Watts, R., and Dainty, R. J. The composition, energy content and function of the stomach oils of petrels (order, procellariiformes) *Journal of Experimental Marine Biology and Ecology* 23 1-13, 1976.

Watts, R. and Warham, J. Structure of some intact lipids of petrel stomach oils *Lipids* 11 423-429, 1976.

Wickham, H., Averick, M., Bryan, J., Chang, W., McGowan, L. D. A., François, R., Grolemund, G., Hayes, A., Henry, L., and Hester, J. Welcome to the Tidyverse *Journal of Open Source Software* 4 1686, 2019.

Xavier, J. C., Raymond, B., Jones, D. C., and Griffiths, H. Biogeography of Cephalopods in the Southern Ocean Using Habitat Suitability Prediction Models *Ecosystems* 19 220-247, 2016.

Xiao, W., Esper, O., and Gersonde, R. Last Glacial - Holocene climate variability in the Atlantic sector of the Southern Ocean *Quaternary Science Reviews* 135 115-137, 2016.

Zhou, L., Heuzé, C., and Mohrmann, M. Early Winter Triggering of the Maud Rise Polynya *Geophysical Research Letters* 49 e2021GL096246, 2022.